A century of anthropogenic environmental change in tropical Asia: Multi-proxy palaeolimnological evidence from Singapore's Central Catchment

Letisha S Fong[1*], Melanie J Leng[2,3] and David Taylor[1]

[1]Department of Geography, National University of Singapore, Singapore
[2]Centre for Environmental Geochemistry, School of Biosciences, University of Nottingham, UK
[3]National Environmental Isotope Facility, British Geological Survey, UK

*Corresponding author, email: letisha.fong@u.nus.edu

Abstract

The environmental ramifications of rapid development on the functioning of warm tropical freshwater ecosystems are poorly understood. Here, a multi-proxy palaeolimnological approach is used to examine the nature and degree of anthropogenic environmental change in a tropical lowland reservoir in Singapore. Singapore has undergone a dramatic transformation over the past century, transitioning from a country with a largely agrarian landscape to one that is highly urbanised. Two radiometrically-dated sediment cores were retrieved from one of the country's oldest reservoirs and analysed for spheroidal carbonaceous particles (SCPs), mercury (Hg), atomic carbon (C) and nitrogen (N), stable C and N isotopes (δ^{13}C and δ^{15}N), and diatoms. The sedimentary data show clear evidence of atmospheric pollution and nutrient enrichment as a result of human activities in Singapore and the region. During the early stages of Singapore's development (1900s–1960s), the reservoir was minimally impacted and characterised by oligotrophic conditions. As the country began to industrialise and urbanise (1970s–1990s), the SCP data indicate increasing contamination by air pollutants derived from domestic sources of fossil fuel combustion, while the diatom, C/N, δ^{13}C, and δ^{15}N data suggest that the reservoir was becoming more productive, possibly from N depositions arising from an increase in electricity generation and a rapid expansion in transport infrastructure in Singapore. As the pace of development in Singapore slowed down (1990s–the present), the sedimentary data collectively indicate increasing depositions of atmospheric pollutants and nutrient enrichment mediated by a warming climate. A substantial component of increased atmospheric pollution is likely to be of distal, and thus transboundary, origin.

Keywords: Anthropocene, climate change, eutrophication, palaeolimnology, pollution, urbanisation

Introduction

The degradation of freshwater ecosystems has become a global environmental problem, notably since the Great Acceleration of the mid-20th century. The Great Acceleration is characterised by the unprecedented rate of population growth and economic development following World War II, and marks a time when the impact of human activities became discernible at the global scale (Steffen et al., 2015). Since its onset, numerous freshwater ecosystems have been variously impacted by a combination of human-induced stressors including surface water acidification, cultural eutrophication, toxic metal pollution and climate change (Saulnier-Talbot, 2016).

The widespread pollution of freshwater ecosystems has led to a strong push for restoration or at least the implementation of measures aimed at arresting further degradation. From a management perspective, this requires knowledge of the conditions that prevailed prior to significant human impact, the range of natural variability within the ecosystem, and the timing and extent of anthropogenic disturbance that modified its functioning (Saulnier-Talbot, 2016). In the absence of monitoring data of sufficient quality and/or duration, palaeolimnology offers a valuable means of obtaining such information (Smol, 2010). Palaeolimnology involves using the physical, chemical and biological information preserved in undisturbed sediments to reconstruct and evaluate past conditions and processes occurring in and around a lake and its catchment (Last and Smol, 2001), thereby providing evidence that can inform the management and restoration of degraded freshwater ecosystems (Bennion et al., 2015).

While there is a relatively large body of literature examining the impact of human activities on water bodies at temperate and polar latitudes (Jones et al., 2014; Rühland et al., 2015), effects on the functioning of freshwater ecosystems in the tropics remain poorly understood (Bannister et al., 2019). Freshwater ecosystems in the warm tropics, in particular, are characteristically different from their cooler climate equivalents. They are, for instance, more sensitive to increases in nutrient availability because of more efficient nutrient recycling combined with higher ambient temperatures and greater stability in solar irradiance at or near the equator (Lewis, 1996). Nitrogen (N) also tends to be the limiting nutrient for phytoplankton in the tropics as opposed to phosphorus (P) at higher latitudes (Talling and Lemoalle, 1998).

Consequently, management strategies developed for temperate ecosystems may not be directly transferable to tropical ecosystems.

This paper employs a multi-proxy palaeolimnological approach in examining the nature and degree of anthropogenic environmental change in lowland tropical Asia. Singapore, the focus of the study, is a low-lying island city-state in Southeast Asia that has undergone dramatic land-use and land cover changes in the past century. Within the span of a few decades, the country has transformed from one with a largely agrarian landscape and dependent on entrepôt trade to a highly urbanised global metropolis. This transformation was perhaps most dramatic between the 1970s and the 1990s, during which there was a rapid expansion of built-up areas for residential estates, industrial and commercial use, and transportation infrastructure (Figure 1; Wong and Yap, 2004).

In addition to pollution pressures arising from island-wide changes in land-use and land cover, Singapore is also subject to transboundary atmospheric pollution from the region because of its close proximity to the industrialising parts of neighbouring Malaysia and Indonesia (Figure 2a). Southeast Asia currently has one of the fastest rates of urbanisation in the world (Koplitz et al., 2017) and this has resulted in considerable atmospheric pollution produced from mobile sources (e.g. vehicular emissions; Lasko et al., 2018), stationary sources (e.g. power generation plants; Engels et al., 2018) and open burning sources (e.g. forest and peatland fires; Karthik et al., 2017). Many of the pollutants emitted from these sources have considerable residence times in the atmosphere and are capable of travelling long distances before settling via wet and/or dry deposition (Chen and Taylor, 2018). An example is that of biomass burning, which has been a major and recurring problem in the region. These fires are largely associated with deforestation and changing land-use practices, and have become more frequent, intense, and widespread in recent decades, particularly on the Indonesian islands of Kalimantan and Sumatra (Page et al., 2009). The resulting haze pollution has the potential to spread throughout the region and has, on many occasions, affected the economies and health of people living in Indonesia, Brunei, Malaysia, Thailand, and Singapore (Lee et al., 2016). Consequently, countries like Singapore that are not directly involved in pollution-generating activities or that have implemented and enforced regulations to curb emissions can still bear a considerable brunt of the environmental, ecological, and human health impacts of pollutive activities in neighbouring countries. The extent of these impacts relative to those arising from local pollution sources, however, remains unknown.

Great disparities in levels of urbanisation remain among Southeast Asian nations, from Cambodia where little over 20% of the population resides in urban areas to Singapore, with its entirely urbanised population (United Nations Population Division, 2018). Despite the rapid growth in cities and the prospect of continued growth into the future, there is very little understanding of the immediate ecological impacts of rapid development in the tropics, and in Southeast Asia in particular. This paper therefore contributes to improved understanding, by providing the first detailed history of aquatic environmental impacts of urbanisation and industrialisation in Singapore and the region. While no natural lakes exist in Singapore, sediments accumulating in the country's reservoirs potentially contain information on the nature and extent of environmental and ecological changes associated with the relatively recent transformation of Singapore. This paper adopts a multi-proxy approach applied to range of evidence, including two radiometrically-dated sediment cores retrieved from one of the oldest reservoirs in the country. Locations of the two cores were selected in order to accommodate within-basin differences in aquatic environmental pressures and their effects. The proxies studied comprise spheroidal carbonaceous particles (SCPs), mercury (Hg), atomic carbon (C) and N along with their stable isotopes (δ^{13}C and δ^{15}N), and diatoms.

Study area

Little variation exists in climatic conditions across Singapore because of its relatively small size and limited topographic variability. The island city-state has an equatorial climate characterised by abundant rainfall and high and uniform temperatures all year round. While there are no distinct wet and dry seasons, Singapore's climate is strongly influenced by the Asian monsoon regime (Figure 2a). The northeast monsoon, which prevails from December to early March, accounts for about half of the total annual rainfall Singapore receives while the southwest monsoon, which dominates from June to September, is generally associated with warmer and drier days (Singapore National Environment Agency, 2009). In between the monsoonal months are two inter-monsoon periods (April–May and October–November) which are characterised by intermittent rain and light and variable winds.

The study site is an impounded reservoir situated in Singapore's Central Catchment Nature Reserve (Figure 2). It is a shallow, lowland (*c.* 18 m a.s.l.) freshwater reservoir with a maximum depth of 9 m and receives water mainly from rainfall, small streams flowing through the protected reserve, and surface runoff from a nearby golf course and recreational park. The reservoir was constructed on a former swampland in the late 19th century (Yeo and Lim, 2011)

and is currently set in a catchment dominated by primary dipterocarp and old secondary rainforest (Wong et al., 1994). Catchment soils are ultisols, which overlie a range of deeply weathered plutonic rocks known as Bukit Timah granite (Wong et al., 1994).

Methods

Sediment coring

Two sediment cores were collected from the reservoir in June 2017 using a UWITEC gravity corer with an inner diameter of 86 mm. The master core (MRR2; 68 cm long) was analysed for all proxies described here and was retrieved from the centre of the reservoir (water depth = 5 m). A supplementary core (MRR1; 43 cm long) was analysed for organic matter content, SCPs and diatoms, and was retrieved from the eastern part of the reservoir (water depth = 6.9 m). Both cores preserved their sediment–water interface and were subsampled at contiguous 1-cm intervals in the field. The samples were then transported to the National University of Singapore (NUS) and refrigerated until subsequent laboratory analyses.

Soil sampling

Deep soil samples were taken from the forested catchment of the reservoir to determine the natural background concentration of Hg in the nature reserve and to assist in the interpretation of Hg levels in the sediment core samples. Soil samples were collected in areas with little or no human access and at a depth below the level expected to be affected by anthropogenic sources of Hg. A standard open-face soil auger was used to obtain eight samples at depths ranging from 50 to 70 cm below the soil surface and at different elevations to account for possible variations in soil properties along a catena.

Radiometric ^{210}Pb dating

Chronological analysis for both MRR2 and MRR1 was carried out at the University College London (UCL) Environmental Radiometric Facility. A total of 14 samples from MRR2 and 17 samples from MRR1 were air-dried and analysed for ^{210}Pb, ^{226}Ra, and ^{137}Cs by direct gamma assay using an ORTEC HPGe GWL series well-type coaxial low background intrinsic germanium detector. ^{210}Pb was determined through its gamma emissions at 46.5 keV and ^{226}Ra by the 295 and 352 keV gamma rays emitted by its daughter isotope ^{214}Pb following 3 weeks of storage in sealed containers to allow for radioactive equilibration. ^{137}Cs was measured by its gamma emissions at 662 keV (Appleby et al., 1986). Chronological control was assisted by

known dates of reservoir construction and subsequent enlargement, as these provide an absolute maximum age for the base of the sedimentary record.

Sediment lithostratigraphy

Loss-on-ignition (LOI) analysis was performed on every sediment core sample to estimate their organic matter content using the procedure outlined in Dean (1974). This involved combusting a known amount of dried material in a furnace at 550°C.

SCPs

SCPs are fine particulates produced from the incomplete combustion of fossil fuels at high temperatures (Rose, 2015). As they have no natural sources, SCPs serve as unambiguous indicators of anthropogenic atmospheric contamination and have been used to reconstruct the history and intensity of atmospherically deposited pollutants from the industrial-scale combustion of fossil fuels (Rose, 2015). Analysis of SCPs was undertaken at 2-cm intervals in both sediment cores following the protocol by Rose (1994). Oven-dried subsamples were sequentially treated with HNO_3 and HCl to remove organic and carbonate materials, respectively. HF was excluded from the digestion sequence for safety reasons. This did not affect the final results as SCP concentrations for both cores fell well within the typical detection limit of 50–80 gDM^{-1} (Rose, 1994). A known fraction of the resulting suspension was evaporated onto coverslips and mounted onto microscope glass slides. SCPs were counted at ×400 magnification using a light microscope and identified following the reference standard developed by Rose (2008). SCP concentrations were calculated as the number of particles per gram of dried sediment (gDM^{-1}) and converted to fluxes (no. cm^{-2} yr^{-1}) to account for variations in sediment accumulation rates.

Mercury

Emissions of Hg from anthropogenic sources have tripled globally since preindustrial times as a result of increased coal combustion, ore refining, waste incineration and metal production (Yang et al., 2016). Hg is one of the most toxic elements, with a tendency to bioconcentrate and bioaccumulate through the food web, hence increasing the risks to human and ecosystem health (Swain et al., 2007). In spite of this, there is little information on past levels of Hg pollution in East and Southeast Asia, a region currently responsible for the highest Hg emissions globally (United Nations Environment Programme, 2019). Analyses of Hg were

carried out on 16 samples from MRR2 and 8 catchment soil samples at the UCL Environmental Change Research Centre. Dried samples were digested with 8 mL aqua regia in acid-leached polypropylene tubes and heated on a hotplate at 100°C for 2 h along with standard reference materials and sample blanks. Upon cooling, the digested solutions were diluted with deionised water and analysed for Hg using cold vapour-atomic fluorescence spectrometry following reduction with $SnCl_2$(Yang et al., 2016). The standard reference material stream sediment GBW07305 used has a certified Hg value of 100 ± 10 ng g^{-1} with a measured mean of 103.6 ng g^{-1} and relative standard deviation of 3.9 ng g^{-1} for sedimentary Hg analyses, and a measured mean of 105.8 ng g^{-1} and relative standard deviation of 1.1 ng g^{-1} for soil Hg analyses.

Carbon and nitrogen

The amount of sedimentary organic matter originating from aquatic and terrestrial plants has often been distinguished based on the ratio of atomic C to N (C/N; Meyers, 1994), while the source(s) of this matter can potentially be deduced from levels of the stable isotopes $\delta^{13}C$ and $\delta^{15}N$ (Leng et al., 2006). Analyses of C and N were undertaken on 50 samples from MRR2 in the Stable Isotope Facility at the British Geological Survey, UK. Samples for C isotopes were decarbonated in 5% HCl prior to analysis to remove inorganic C, while a separate aliquot for N isotopes was run with no pretreatment. $\delta^{13}C$ analyses were performed by combustion in a Costech ECS4010 Elemental Analyser online to a VG TripleTrap (plus secondary cryogenic trap) and Optima dual-inlet mass spectrometer, with $\delta^{13}C$ values calculated to the VPDB scale using a within-run laboratory standard (BROC2) calibrated against NBS-19 and NBS- 22. %C and %N analyses were run concurrently and calibrated against an Acetanilide standard. In addition, $\delta^{15}N$ analyses were performed by combustion in a Thermo Finnigan Flash Elemental Analyser (1112 series) online to a Delta Plus XL mass spectrometer, with $\delta^{15}N$ values calculated to the $\delta^{15}N$ value of air using the BROC2 standard as a within-run laboratory standard calibrated against UGS40 and UGS4a. Replicate analysis of well-mixed samples indicated a precision of ± <0.1 for C/N, ± 0.1‰ (1 SD) for $\delta^{13}C$ and ± <0.2‰ (1 SD) for $\delta^{15}N$.

Diatoms

Diatoms (Bacillariophyceae) are a group of unicellular algae that have been extensively used in tracking past aquatic environmental changes because of their sensitivity to changes in water quality (Smol and Stoermer, 2010). Diatom analysis was undertaken at 1-cm intervals in MRR2 and 2-cm intervals in MRR1 following standard procedures (Battarbee, 1986; Renberg, 1990).

Wet sediment samples were treated with 10% HCl to remove carbonate materials and 20% H_2O_2 to oxidise all organic matter. After diluting the processed sample, the final suspension was evaporated onto coverslips and mounted onto microscope glass slides. At least 300 valves per sample were identified and enumerated under oil immersion phase contrast light microscopy at ×1000 magnification. Diatom taxonomy followed a variety of general (Krammer and Lange-Bertalot, 1986, 1988, 1991a, 1991b; Lange-Bertalot et al., 2017), genus-specific (Krammer, 2000; Lange-Bertalot et al., 2011; Lange-Bertalot and Moser, 1994) and online (Diatoms of North America; diatoms.org; AlgaeBase; algaebase.org; European Diatom Database (EDDI); craticula.ncl.ac.uk/Eddi) floras. Valve dissolution was assessed using a binary classification system and encapsulated in the *F* index (Ryves et al., 2006), while diatom concentrations were derived from diatom abundances by adding a known concentration of microspheres to each sample (Battarbee and Kneen, 1982). The diatom data are expressed as percentage relative abundances and as fluxes (no. cm^{-2} yr^{-1}).

Numerical analyses

All statistical analyses were performed in the R language and environment (R Core Team, 2018). Diatom data were divided into assemblage zones using constrained incremental sum of squares cluster analysis (CONISS; Grimm, 1987) and the number of significant and potentially useful zones identified by comparing the clustering results with the broken-stick model (Bennett, 1996). Redundancy analysis (RDA) was carried out to determine whether there was a driver–response relationship between SCP fluxes and diatoms. Linear ordination was deemed appropriate as exploratory detrended correspondence analysis (DCA) on all taxa ≥1% abundance in any one sample revealed a gradient of 1.83 SD and 2.12 SD for MRR2 and MRR1, respectively.

Reconstructions of diatom-inferred total phosphorus (DI-TP) were produced using the combined TP training set comprising 347 European lakes from the EDDI database (Battarbee et al., 2000). The EDDI database was used as there is currently no regional TP training set for Southeast Asia. The two best models were generated with (1) weighted-averaging (WA) regression and calibration with tolerance down-weighting and classic deshrinking, and (2) the modern analogue technique (MAT), and both were internally cross-validated via bootstrapping with 1000 permutations. The use of transfer functions to infer past variations in water quality has received much criticism of late because of the common violation of several key assumptions (Juggins, 2013). Here, we acknowledge that the accuracy of the DI-TP

reconstructions may be affected as (1) the training set is unlikely to fully accommodate the range of environmental conditions represented in the sediment cores—only 47% and 57% of diatom species in MRR1 and MRR2, respectively, were represented in the training set, (2) there are no accessible instrumental records of epilimnetic TP to assess and validate the reconstructions and (3) it is unlikely that up-core changes in diatom composition are solely driven by TP and are instead responses to a combination of chemical and limnological variables that are in turn a product of the interactions between climate, catchment and in-lake processes (Juggins and Birks, 2012). Both the WA and MAT models were considered in this study as the reconstructions followed similar trajectories despite differing in inferred values. While this limits the discussion of absolute values, the trending similarities suggest that both models are free from technique-specific bias (Köster et al., 2004) and so fluctuations in the abundances of dominant taxa are, at least in part, related to changes in TP (Juggins and Birks, 2012). Notwithstanding the above limitations, since the focus of this paper is to examine the nature of anthropogenic aquatic impacts more broadly, both the WA- and MAT-based reconstructions are referred to in combination with other sources of evidence.

Historical temperature data

Climatic changes exert strong moderating controls on many lake processes, which can directly or indirectly alter the population dynamics of phytoplankton, including diatoms (Arnell et al., 2015). Recent climate warming has, in particular, been implicated in the crossing of ecological thresholds in many freshwater ecosystems (Rühland et al., 2015). Secondary data on past variations in surface air temperature were used to test for possible relationships between up-core changes in diatom species abundances and climate warming. Historical climate data for Singapore in the form of mean monthly surface air temperatures over the time period AD 1901–2015 were obtained from the World Bank Climate Change Knowledge Portal (climateknowledgeportal.worldbank.org) and used to determine mean annual surface air temperature anomalies, or the difference between annual temperature and the long-term mean. Past variations in the annual total precipitation were not included in the interpretation of data as there were no abnormal rainfall patterns or significant deviations from the long-term mean from AD 1901–2015 (Supplementary Figure 1, available online).

Results

Core chronology and sediment accumulation rates

The constant rate of supply (CRS) dating model (Appleby and Oldfield, 1978) was used to derive the chronologies and sediment accumulation rates for both sediment cores, as the decline in unsupported ^{210}Pb activities was non-monotonic (Supplementary Figures 2 and 3 and Supplementary Tables 1 and 2, available online). In MRR2, the CRS model dates the basal sediments (67–68 cm) to AD 1913 ± 16 years, with sediment accumulation rates gradually increasing from *c.* 0.12 g cm^{-2} yr^{-1} at the base of the core to *c.* 0.31 g cm^{-2} yr^{-1} in the mid-1990s. Thereafter, rates were relatively constant, averaging around 0.20 g cm^{-2} yr^{-1}. ^{137}Cs activities were detected at two isolated depths but at levels too low to be useful for dating.

For MRR1, sediment accumulation rates in the upper 17 cm varied between 0.05 and 0.10 g cm^{-2} yr^{-1}. Below 17 cm, unsupported ^{210}Pb activities are low and the errors considerable; the confidence in assigning dates to this section of the core is therefore low. The sediment accumulation rate profile and distinct changes in sediment properties suggest that the sedimentary record was disturbed around 19 cm. A likely cause of this disturbance is enlargement works that were carried out at the study site in the late 19th and early 20th centuries (Yeo and Lim, 2011). As MRR1 is located in what was originally an area of freshwater swamp between the former embankment and the current dam, sediments deposited below 19 cm may have been disturbed by in-wash associated with the enlargement works, comprise the peaty substrate from the freshwater swamp or some combination of the two. Because of these reasons, and because the LOI, SCP and diatom data in the upper part of MRR1 (19–0 cm) exhibit similar trends with MRR2 (Figure 3), only the ^{210}Pb-derived dates and sediment accumulation rates between 0 and 17 cm of MRR1 are referred to in this paper. Sediments at 19 cm were not radiometrically dated and presumably date to the period during and/or just after enlargement works were carried out (early 1900s). As no ^{137}Cs activity was detected in the analysed samples, the chronology of MRR1 has not been validated by an independent time marker and any interpretations made are treated with caution.

Sediment lithostratigraphy

The LOI results indicate that the composition of sediments in MRR2 was generally uniform throughout the core (Figure 3). By comparison, sediment composition in MRR1 was much more variable (Figure 3). In MRR2, the organic matter content was relatively stable and fluctuated between 16% and 21%, although there was a slight increase in values above 41.5

cm (AD 1966 ± 7 years). This uniformity is reflected in the physical characteristics of the sediments, which comprised dark greyish-brown material with a soft and clayey-silt texture. In MRR1, LOI values ranged between 16% and 40%, with sediments between 43 and 32 cm having a relatively high organic matter content (33–40%). Thereafter, the values decline to 19% at 19 cm before stabilising around a mean of 18 ± 2% between 19 and 0 cm (throughout the 20th century). Sediments in the upper part of MRR1 (19–0 cm) were similar in colour and texture to those of MRR2, but became darker in colour and coarser in texture below 19 cm. This lower section also had a high abundance of plant remains comprising roots, leaves, wood and charcoal fragments. When comparing the LOI profiles of both cores, the upper profile of MRR1 (19–0 cm) correlates well with the full profile of MRR2. Figure 3 illustrates this by identifying points where the two cores exhibit similar magnitudes of and changes in organic content, and are of approximately the same age.

SCPs

The three main features that typically characterise SCP profiles—(1) the start of the particle record, (2) the rapid increase in particle accumulation and (3) the peak and subsequent decline in particle concentrations and fluxes—are present in both sediment cores, but the absolute fluxes between them differ considerably, with values ranging from 1000 to 42,000 no. cm^{-2} yr^{-1} in MRR2 (Figure 4) and 300–8700 no. cm^{-2} yr^{-1} in MRR1 (Figure 5). In MRR2, the first appearance of SCPs pre-date the period covered by the core, with SCP fluxes rising slowly from about 1000 no. cm^{-2} yr^{-1} in AD 1913 ± 16 years to 7400 no. cm^{-2} yr^{-1} in AD 1955 ± 9 years. Thereafter, SCP fluxes increase markedly before peaking around AD 1987 ± 4 years. While there was a decline in particle accumulation from the late 1980s, SCP fluxes begin to rise again towards the top of the core around the early 1990s, albeit at a lower rate. In MRR1, single appearances of SCPs occur between 27 and 20 cm in the core (dating to the early 20th century or earlier). A rapid increase in SCP fluxes occurs around 14.5 cm (AD 1951 ± 10 years) followed by a peak in the late 1990s.

Sedimentary and soil Hg

Levels of Hg in the basal sediments of MRR2 recorded a concentration of 201 ng g^{-1} and flux of 231 μg m^{-2} yr^{-1} (Figure 4). Hg fluxes increased steadily from AD 1913 ± 16 years to peak at a value of 659 μg m^{-2} yr^{-1} around the mid-1970s, following which they decline to a low of 232 μg m^{-2} yr^{-1} in AD 1994 ± 3 years before rising again towards the top of the core where values reach as high as the first peak (658 μg m^{-2} yr^{-1}). The analysis of deep soil Hg revealed

that the mean Hg concentration of the eight soil samples is 97 ng g^{-1}, with sample 3B recording the highest (232 ng g^{-1}; Figure 6) and sample 3A recording the lowest (21–24 ng g^{-1}; Figure 6) values. The latter sample was processed twice to confirm the low concentration.

Carbon and nitrogen

Up-core changes in C/N ratios were relatively modest and varied from 10.1 to 13.0 (Figure 4). The ratios generally begin to decline from AD 1963 ± 8 years, becoming progressively lower towards the top of the core. The profile of $\delta^{13}C$ was largely synchronous with the C/N ratios, with values ranging from −24.9‰ to −26.1‰ between AD 1913 ± 16 years and AD 1963 ± 8 years, after which it declines to a low of −29.2‰ at the surface (Figure 4). $\delta^{15}N$ generally increased throughout the length of the core from +1.9‰ in the basal sediments to +3.0‰ at AD 1963 ± 8 years (Figure 4). Thereafter, $\delta^{15}N$ declines by about 0.5‰ up until the mid-1980s, where the values stabilise and fluctuate around a mean of +2.4‰.

Diatoms

A total of 58 species from MRR2 and 65 species from MRR1 were recorded (see Supplementary Table 3 for a full list of taxonomic names and authorities, available online). The clustering results identified four assemblage zones for MRR1 (Figure 5) and three assemblage zones for MRR2, with Zone 1 of MRR2 further divided into two subzones (Figure 4). The zones are in reasonable agreement between the two cores in terms of the nature and timing of floristic shifts: Zone 2 of MRR1 (early 1900s–AD 1951 ± 19 years) corresponds to Zone 1a of MRR2 (AD 1913 ± 16 years–AD 1963 ± 8 years), Zone 3 of MRR1 (AD 1951 ± 19 years–AD 1979 ± 4 years) corresponds to Zone 1b of MRR2 (AD 1963 ± 8 years–AD 1978 ± 5 years) and Zone 4 of MRR1 (AD 1979 ± 4 years–AD 2017 ± 2 years) corresponds to Zones 2 and 3 of MRR2 (AD 1978 ± 5 years–AD 2017 ± 2 years).

Diatoms were absent below 30 cm in MRR1 and were found in very low abundances between 30 and 19 cm of the core where sediments are presumably disturbed. This section of the core (Zone 1) is the only zone where aerophilous *Luticola* taxa, which constitute *c.* 20% of the total assemblage composition, are present, thereby supporting the earlier suggestion that sediments deposited below 19 cm are likely sourced from the freshwater swamp that became part of the enlarged reservoir in the late 19th and early 20th centuries.

Throughout the first half of the 20th century (Zone 2 of MRR1; Zone 1a of MRR2), the sedimentary record is predominated by the benthic diatoms *Frustulia saxonica* Rabenhorst, *Brachysira brebissonii* R. Ross, *Brachysira neoacuta* Lange-Bertalot and *Kurtkrammeria lacusglacialis* (L. Bahls). Valve preservation is generally poor (*F* index <0.5) and is at its lowest in these zones. Here, the valves of *F. saxonica* were appreciably dissolved and/or broken except for the characteristic thickened portion containing the raphe. Diatom fluxes for both cores are relatively low as well. Reconstructed DI-TP levels are stable throughout this time period and generally fall in the oligotrophic (<10 μg L^{-1}) range (OECD, 1982).

The assemblage continues to be predominated by *F. saxonica* between the mid-20th century and the late 1970s (Zone 3 of MRR1; Zone 1b of MRR2), although the planktonic taxa *Aulacoseira granulata* (Ehrenberg) Simonsen and *Discostella* complex comprising *D. stelligera* (Cleve & Grunow) Houk & Klee and *D. pseudostelligera* (Hustedt) Houk & Klee begin to occur in low abundances. Diatom fluxes begin to increase slightly from the early 1970s, with reconstructed epilimnetic TP concentrations falling in the oligotrophic to mesotrophic (10–30 μg L^{-1}) range. Valves are generally more well preserved in these zones.

There is a clear shift in the composition of the diatom assemblage from the early 1980s onwards (Zone 4 of MRR1; Zones 2 and 3 of MRR2). *Frustulia saxonica* declines to its lowest abundance in both cores and is gradually replaced by *A. granulata, Discostella* complex and *Brachysira neoexilis* Lange-Bertalot. This shift is accompanied by an increase in the ratio of planktonic to benthic diatoms and in the fluxes of diatoms. In addition, the DI-TP values indicate a departure from previously stable TP levels towards that of increasing productivity.

Diatom response to changes in SCP fluxes

RDA identified SCP flux as a significant and important driver of diatom response in both sediment cores, with *p* value estimates of 0.001 and correlation coefficients of −0.69 and −0.86 for MRR2 and MRR1, respectively. The RDA biplot for MRR2 indicates that SCP fluxes were positively associated with the diatoms *A. granulata, B. neoexilis* and *D. pseudostelligera* and negatively associated with *F. saxonica, B. brebissonii* and *B. neoacuta* (Supplementary Figure 4a, available online). Likewise, the biplot for MRR1 shows that SCP fluxes were positively associated with *D. pseudostelligera* and *A. granulata* and negatively associated with *F. saxonica* (Supplementary Figure 4b, available online).

Surface air temperature anomalies

Historical surface air temperature anomalies for Singapore are presented in Figure 4. Between AD 1901 and 1982, temperature anomalies were predominantly negative (mean of −0.19°C), indicating that the ambient environment was cooler than the long-term average. The anomalies were subsequently positive through to AD 2015, fluctuating around a mean of +0.46°C.

Discussion

Early stages of development: Minimally impacted conditions

Prior to the onset of rapid industrialisation and urbanisation in Singapore in the 1970s, diatom assemblages at the study site displayed negligible floristic change and comprised taxa typically associated with nutrient-poor and naturally acidic to circumneutral conditions. The three most abundant species, *F. saxonica, B. brebissonii* and *B. neoacuta*, are acidophilous taxa commonly found in waters with good ecological quality (Lange-Bertalot et al., 2017; Van Dam et al., 1994), while *K. lacusglacialis*, which is also present throughout this period, tends to thrive in oligotrophic environments with a pH ranging from 6.5 to 7.6 (Bahls, 2013, 2015). The predominant occurrences of these taxa along with the low diatom fluxes and DI-TP concentrations in both cores indicate that the reservoir was a relatively unproductive system. A largely stable diatom community coupled with low productivity levels is characteristic of constructed reservoirs that have not been subject to subsequent nutrient loading following their completion (e.g. Donar et al., 1996; Marsicano et al., 1995), and supports the reservoir development hypothesis, which posits that artificially dammed reservoirs generally undergo a period of trophic upsurge immediately following their formation, after which conditions stabilise and a phase of trophic depression ensues (Kimmel and Groeger, 1986). Thereafter, the trophic status of a reservoir is largely dependent on the degree of catchment disturbance or other anthropogenic sources of nutrient enrichment. Zone 2 of MRR1 (early 1900s–AD 1951 ± 10 years) and Zone 1a of MRR2 (AD 1913 ± 16 years–AD 1963 ± 8 years) could therefore represent a prolonged trophic depression phase, with small fluctuations in diatom abundances around a relatively stable mean likely representing the historical long-term variability of the study site in the absence, or minimal presence, of significant human impact (Mills et al., 2017).

SCP flux data show relatively low particle accumulation rates in both MRR1 and MRR2, with fluxes rising gradually from the early 20th century through to the early to mid-1950s. This increase is contemporaneous with global SCP records and typically represents the early use of coal for power generation (Rose, 2015). The low accumulation of SCPs at the

study site likely reflects emissions from St James Power Station, Singapore's first (commissioned in AD 1926) and at the time only operating power station located in the southern part of the island. In terms of absolute values, while SCP depositions are generally higher at the study site compared with most lakes around the world (Rose, 2015), fluxes up to the rapid rise in the mid-1950s are comparable with those recorded in relatively remote lakes in Scotland (e.g. Round Loch of Glenhead; Rose and Appleby, 2005) and Canada (e.g. Cold Lake; Reinemann et al., 2014).

There is evidence of elevated levels of Hg at the study site dating to Singapore's pre-industrialisation and urbanisation phase. The Hg flux in the basal sediments of MRR2 are considerably higher (231 μg m^{-2} yr^{-1}) than pre-industrial Hg fluxes recorded in other parts of the world, which generally fall below 50 μg m^{-2} yr^{-1} (e.g. Engstrom et al., 2014; Reinemann et al., 2014; Yang et al., 2016). The mean concentration of Hg (*c.* 206 ng g^{-1}) in sediments deposited prior to the 1960s is also higher than the average concentration of Hg in the Earth's upper continental crust (50 ng g^{-1}; Rudnick and Gao, 2013) and the consensus-based sediment quality guideline on the threshold effect concentration of Hg (180 ng g^{-1}; MacDonald et al., 2000). Analyses of soil Hg revealed a comparatively thick horizon containing elevated levels of Hg in all samples tested except for sample 3A, in which the concentration of Hg was relatively low and ranged between 21 and 24 ng g^{-1}. These low values are comparable to the levels of Hg typically associated with soils overlying bedrock of granitic origin (30 ng g^{-1}; Yang and Rose, 2003) and likely represent the natural background level of Hg in forest-covered soils of the Central Catchment Nature Reserve. In the absence of industrial-scale coal combustion, oil refining and cement production—all of which are modern sources of Hg emissions (United Nations Environment Programme, 2019)—in Southeast Asia prior to the 20th century, and by ruling out naturally elevated levels of Hg in the reservoir's catchment, the contamination observed in MRR2 can be attributed to the long-range atmospheric transport of Hg from artisanal and small-scale gold mining activities in Malaysia, particularly in the states of Pahang and Sarawak (Warnford-Lock, 1907). The use of Hg in artisanal and small-scale mining has taken place for thousands of years as it is a relatively simple and cheap means of extracting gold (Gworek et al., 2017). The location of Singapore just downwind of Pahang (*c.* 140 km) with respect to the northeast monsoonal winds suggests that emissions from mining activities in Malaysia in the 19th century could have contributed to elevated levels of Hg at the study site during the early stages of development in Singapore.

Rapid industrialisation and urbanisation: Peak in local sources of pollution

The period of rapid industrialisation and urbanisation in Singapore spanned the early 1970s to the 1990s. During this time, the SCP profiles of both sediment cores indicate a transition from low levels of contamination to greatly enhanced particle deposition in the form of a rapid increase in fluxes. This increase, which commenced in the early 1950s, coincides with the opening of four new power stations in Singapore between AD 1953 and 1977 (Lau, 1988) and suggests that the majority of SCPs deposited at the study site during this period originated from domestic sources of fossil fuel combustion. The timing of the rapid increase in SCP fluxes is also concomitant with many other indicators of the Great Acceleration, including primary energy use (Steffen et al., 2015), and is in good agreement with records from other parts of the world; a globally synchronous and rapid increase in SCP accumulation is evident from around AD 1950 in sediment records from 76 lakes distributed across a wide geographical range (Rose, 2015).

Although the timing of the rapid increase in SCP fluxes appears to be globally consistent, there is much greater geographical variability in the timing of when levels peak, occurring around AD 1970 in North America (Charles et al., 1990; Reinemann et al., 2014), AD 1980 in Europe (Rose, 2015; Rose and Appleby, 2005), AD 1990 in Russia and East Asia (Nagafuchi et al., 2009; Rose et al., 2004) and AD 2000 in Southeast Asia (Engels et al., 2018). These differences are, in large part, a reflection of variations in the rates of development and in the effectiveness of measures aimed at curbing pollution (Rose, 2015). Efforts to mitigate environmental pollution began relatively early on in Singapore's industrial and urban transition. Following the initial implementation of the Clean Air Act in AD 1971, newly commissioned power stations were fitted with electrostatic precipitators and tall multi-flue chimneys in the late 1970s, while several of the older power stations ceased operations through the 1980s (Lau, 1988; Ng and Lung, 1985). Considered together, the timing of the implementation of these measures coincides with, and is likely responsible for, the mid-1980s peak in SCP fluxes seen in MRR2. The 10-year delay observed in MRR1 could be a reflection of errors associated with the ^{210}Pb technique or a result of the low temporal resolution of the record, as dry mass sediment accumulation rates are, on average, lower than those of MRR2 by a factor of three. This would have potentially blurred the trends seen in MRR2. The fairly large discrepancy between the maximum flux values of SCPs in both sediment cores—MRR2 has a maximum flux of 42,000 no. cm^{-2} yr^{-1} while MRR1 has peak values of 8700 no. cm^{-2} yr^{-1}—has been observed in some lakes and is thought to result from localised sediment focusing,

although it remains unclear why such considerable differences occur over relatively small distances on a reasonably flat sediment bed (Bindler et al., 2001; Rose et al., 1999).

Between the 1960s and the 1990s, the record of diatoms, atomic C/N ratios and $\delta^{13}C$ suggests that the study site underwent a period of increasing productivity. *Aulacoseira granulata* and *B. neoexilis*, taxa that are generally tolerant of more nutrient-rich conditions, gradually began to replace previously abundant oligotrophic taxa from about AD 1970 onwards. *Aulacoseira granulata* is a cosmopolitan planktonic taxon commonly associated with mesotrophic to highly eutrophic waters (Bicudo et al., 2016; Van Dam et al., 1994), while *B. neoexilis* is often found in mesotrophic habitats and is known to be more tolerant of nutrient loading compared with other species in its genus (Lange-Bertalot et al., 2017; Lange-Bertalot and Moser, 1994). Increasing abundances of *A. granulata*, in particular, are largely driving up-core variations in diatom fluxes and planktonic/benthic ratios. In addition, DI-TP concentrations depart from the relatively stable levels that characterised the pre-industrialisation and urbanisation phase. These changes reflect an increase in nutrient loading at the reservoir and might provide an early warning or indication that an ecologically important threshold—in the form of deviations from the historical long-term variability—was now being crossed (Battarbee, 1999). Similar findings have been recorded in palaeolimnological studies of Loch Ness and Loch Lomond in the UK, where despite negligible increases in TP and DI-TP levels, there were marked changes in the composition of planktonic diatom flora towards species indicative of nutrient enrichment (Bennion et al., 2004; Jones et al., 1997).

Floristic shifts in the diatom community at the study site occurred around the same time as a decline in C/N ratios and $\delta^{13}C$ values. C/N ratios greater than 20 are generally indicative of a largely terrestrial source of sedimentary organic matter, while those less than 10 are often linked to a predominantly autochthonous source (Meyers, 2003). C/N data suggest that organic material in MRR2 is derived from both terrestrial and aquatic plant sources, although the steady decline in values from 12.9 in AD 1963 ± 8 years towards the uppermost sediments indicates that algae became increasingly prominent contributors to sedimentary organic matter. The inferred enrichment from the diatom and C/N data is further supported by values of $\delta^{13}C$, which range from −25‰ to −30‰ and become progressively negative towards the top of the core. These values and trend indicate a switch in plant type from a mixed source comprising terrestrial and aquatic vegetation to a predominantly algal source.

Given that the observed changes are concomitant with the onset of rapid industrialisation and urbanisation in Singapore, land-use change may have, at least in part, driven an increase in nutrient loading at the reservoir. RDA for both cores indicates that SCP flux was a strong predictor of diatom response at the reservoir. However, whereas SCP flux would normally be expected to be positively correlated with acidophilous taxa because of acidification from industrial sources (Battarbee et al., 2015), the RDA biplots instead reveal a negative association between SCP flux and *F. saxonica* and *B. brebissonii*, both acidophilous and oligotrophic diatoms, but a positive association with *A. granulata, B. neoexilis* and *D. pseudostelligera*, all of which favour more nutrient-rich conditions. This suggests that increasing productivity was a dominant driver of ecological change at the study site, and that any acidification pressures associated with industrialisation were secondary. Since sources of SCPs are also significant sources of nitrogen oxides (Rose, 2001), up-core changes in diatom composition may be attributable to the effects of N enrichment arising from an increase in electricity generation in Singapore. Synchronies between increasing SCP fluxes and the timing of diatom species shifts indicative of eutrophication as a consequence of N depositions from fossil fuel combustion sources have similarly been recorded in remote lakes in Scotland (Pla et al., 2009) and Finland (Korhola et al., 2002).

The potential effects of atmospheric N deposition on lake trophic status have only until recently become a focus of attention, as most freshwater studies have previously focused on the impact of N input on surface water acidification or on eutrophication because of catchment-based activities (Curtis and Simpson, 2007). Although up-core changes in $\delta^{15}N$ are relatively modest in MRR2, there is a slight but notable depletion in $\delta^{15}N$ values by about 0.5‰ from a maximum of +3.0‰ around the mid-1960s to the mid-1980s. This depletion correlates closely with the rapid increase in SCP fluxes, suggesting that N emissions from the expansion of domestic fossil fuel combustion likely accounted for the lower values (Battarbee et al., 2015). Similar trends—both in timing and magnitude—as a response to major increases in the combustion of fossil fuels during the Great Acceleration have been recorded in upland lakes in the UK (Battarbee et al., 2015; Curtis and Simpson, 2007) and in ice cores from Greenland (Hastings et al., 2009). Nevertheless, while N deposition from fossil fuel combustion sources is likely the dominant driver of ecological change at the study site, other potential sources of nutrients that may have promoted productivity include runoff from the redevelopment of a recreational park along the south-eastern edge of the reservoir in the mid-1980s and the

application of synthetic fertilisers to maintain the quality of the golf course turf adjacent to the western edge of the reservoir.

Despite multiple independent lines of evidence indicating anthropogenic nutrient enrichment at the study site in the late 20th century, the level of enrichment observed does not appear to be as marked when compared with places that have undergone similar levels of urbanisation and land-use change. In places where substantial development has taken place, freshwater ecosystems often exhibit a clear and at times abrupt response to anthropogenic nutrient pollution (e.g. Dong et al., 2008; Fontana et al., 2014). In such instances, the primary driver of urbanisation-related eutrophication is typically an increase in N or P loadings from municipal and industrial wastes (Bennion et al., 2015). For Singapore, the discharge of such wastes into waterways feeding into the country's reservoirs was prevented early on by the establishment of a comprehensive sewerage system serving all industrial, residential and commercial premises in AD 1972 (Wong and Yap, 2004) and by the Water Pollution Control and Drainage Act of AD 1975 (Tortajada et al., 2013), shortly after rapid industrialisation and urbanisation in Singapore took off. Nutrient enrichment observed at the study site is therefore not as substantial as one would expect for a reservoir located so close to areas undergoing industrial and urban development. In addition, the continued predominance of *F. saxonica* during this period of industrialisation and urbanisation could be attributed to the long-standing (since the late 19th century) protected status of the reservoir and its forested catchment. This has effectively minimised pollutants flowing into the reservoir, as research on Singapore's other reservoirs, most of which are located in unprotected catchments, indicate that these systems are eutrophic to hypereutrophic and highly susceptible to nutrient enrichment from waterways that run through a predominantly urban setting (Low and Ng, 2010; Yang and Chiam-Tai, 1991).

Highly developed state: Effects of increasing transboundary pollution and climate change

Singapore's rapid urban and industrial transition was more or less complete by the early 1990s, with the World Bank classifying the country as a high-income economy for the first time in AD 1989 (World Bank, 1989). This period was characterised in the sedimentary record by a decline in SCP fluxes that generally corresponds to a tightening of pollution mitigation measures in Singapore. In addition to new and amendments to existing environmental pollution legislation and emissions control technologies, Singapore had also begun switching to cleaner forms of fuel in the late 1980s (Ang, 1994). This was characterised by a reduced dependence

on fuel-oil and the introduction of natural gas as a primary source of energy. By AD 2005, natural gas accounted for 75% of the country's fuel mix and in AD 2017 was responsible for 95% of the total electricity generated in Singapore (Energy Market Authority, 2017).

In spite of these measures, however, the SCP profile of MRR2 shows an increase in SCP depositions towards the top of the core from AD 1997 ± 3 years. Depositions at some lakes in eastern US, northwest Europe and north Africa also show double peaks in SCP fluxes evident in MRR2 (Rose, 2015). This second rise could indicate a predominance of transboundary atmospheric pollution, with the most likely emission sources in neighbouring parts of Indonesia and Malaysia. Records of power stations in these two countries indicate that the majority of the stations only began operations after the mid-1990s (Supplementary Table 4, available online). As many of these power stations also sit in the path of the northeast and southwest monsoons, emissions arising from electricity-generation activities in the region could be carried in the atmosphere before being deposited at the study site (Figure 7). This predominantly transboundary source of pollution is further supported by trends in the sedimentary Hg flux data, which exhibited a second increase from the mid-1990s following the mid-1980s decline. In Southeast Asia, the two largest emission sources of Hg are coal combustion and artisanal and small-scale gold mining (Pacyna et al., 2016; United Nations Environment Programme, 2019), neither of which are practised in Singapore. Given that the recent increase in Hg fluxes is concomitant with increased coal consumption in the region (U.S. Energy Information Administration, 2016) along with a recent rise in amalgamation-based gold production (Gworek et al., 2017), there is strong circumstantial evidence that the study site is being increasingly impacted by transboundary atmospheric pollution.

Diatom assemblages during Singapore's post-industrialisation and urbanisation phase indicate that productivity was at its highest in the century-long sedimentary record. This is reflected in the DI-TP concentrations, which distinctly deviate from levels that characterised the period of pre-significant anthropogenic impact. During this period, *A. granulata* and *B. neoexilis* reach their maximum abundances in both cores, while the prominence of previously abundant oligotrophic taxa, including *F. saxonica*, is much reduced. The cores also record a pronounced increase in the abundance of planktonic *Discostella* taxa, which grow favourably when nutrients are readily available (Saros and Anderson, 2015; Wengrat et al., 2018). The overall increase in the quality of valve preservation in these zones suggests that dissolution

cannot account for the decline in the abundances of *F. saxonica*, and so the floristic changes are most likely taking place as a response to changes in water quality.

Given the relatively stable sediment accumulation rates and organic matter content in the upper sections of both sediment cores as well as the decline in C/N ratios towards the top of MRR2, there is no evidence to suggest that catchment in-wash had contributed to increased levels of primary production. There is also little indication that local sources were responsible, as the nutrient enrichment seen during the period of rapid industrialisation and urbanisation is not as marked as the present post-industrialisation and urbanisation phase. A possible source of enrichment is the emission of N compounds from development-related activities in the region and from biomass burning. Biomass burning has come to the forefront of environmental issues in Southeast Asia, particularly since the 1990s, because of the scale and extent of the resulting haze pollution. Forest fires emit considerable amounts of reactive N compounds into the atmosphere (Benedict et al., 2017), which can result in nutrient enrichment of aquatic ecosystems upon deposition. A recent study showed that forest and peat fires in Sumatra and Kalimantan were a significant source of atmospheric nutrients to Singapore's marine environment, with the average concentrations of nutrients (N and P species) rising by a factor of 3–8 on hazy days compared with non-hazy days (Sundarambal et al., 2010). This was, however, not apparent in the $\delta^{15}N$ data, which fluctuate around a mean of +2.4‰ from the early 1990s to the present. Although the $\delta^{15}N$ signature of biomass burning is relatively enhanced (Dunnette et al., 2014) and increased deposition of N from biomass burning might therefore be expected to result in increasingly positive sedimentary values, $\delta^{15}N$ from the combustion of fossil fuels tends to be relatively depleted (Felix et al., 2012; Wang et al., 2017). Abundant depositions from both sources could therefore result in little variation in bulk sedimentary $\delta^{15}N$. The relatively large rise in diatom productivity from around AD 2000 may have additionally been linked to a change in the management of the study site, particularly in abandoning the use of copper sulphate as an algaecide to control cyanobacteria blooms in the reservoir between the early 1980s and the late 1990s (Chen et al., 2016).

Recent climate warming has exerted a strong influence on the functioning of many freshwater systems around the world and led to ecological tipping points favouring the growth of small planktonic diatoms (Rühland et al., 2015). One notable feature of the diatom assemblage at the study site is an increased abundance of *Discostella* complex from the 1980s. This coincides with positive mean annual surface air temperature anomalies for Singapore

since AD 1985, and is in line with recent warming-related increases in the occurrences of small centric *Discostella* taxa in lakes located in the Northern Hemisphere (e.g. Rühland and Smol, 2005; Wiltse et al., 2016; Yan et al., 2018) and in a cluster of deep, low-altitude crater lakes in tropical East Asia (Bannister et al., 2019). Nevertheless, given that climate-induced increases in water temperature tend to produce symptoms identical to those created by anthropogenic nutrient enrichment (e.g. increased algal productivity; accelerated nutrient recycling), difficulties arise when attempting to differentiate between the relative role of climate change and nutrient pollution in driving ecological changes (Battarbee et al., 2012; Hobæk et al., 2012). For example, Bennion et al. (2012) reported a coincidence in the presence of *A. granulata* and higher temperatures, while Saros and Anderson (2015) indicated that *Discostella* taxa were responsive to increases in N/P ratios. As the abundances of these diatoms increase with local mean temperature anomalies and at the time of increases in atmospherically derived nutrients from regional biomass burning and development-related activities, higher productivity levels observed at the study site since the early 1990s likely reflect a climate-mediated response to nutrient enrichment and therefore adds weight to the notion that already warm tropical freshwater ecosystems are sensitive to further climate warming.

Authors' note

An existing agreement with the Public Utilities Board (PUB), Singapore's national water agency, precludes disclosure of the name and exact location of the study site, including all sampling points. The authors did not have access to water quality monitoring data and were not authorised to collect modern limnological data for the study site.

Acknowledgements

Thanks are due to the PUB for allowing access to the study site, for providing data where possible, and for facilitating all fieldwork activities. Thanks also to the National Parks Board for allowing access to the soil sampling sites. We would like to thank Chen Qinqin, Wayne Bannister and Joeline Lim for assistance in the field, Elvagris Segovia for assistance in the lab, and Suzanne McGowan, Neil Rose and Handong Yang for helpful advice at different stages of this work. Finally, we are grateful to Viv Jones and two anonymous reviewers for their valuable comments and suggestions on an earlier version of this manuscript.

Funding

This work was supported by the Singapore Ministry of Education through a Tuition Fee Allowance Award to L.S.F. and through a research grant (Grant No. FY2017-FRC1-005).

References

Ang EA (1994) Electricity generation and clean air. *PUB Digest* 15: 20–29.

Appleby PG and Oldfield F (1978) The calculation of lead-210 dates assuming a constant rate of supply of unsupported ^{210}Pb to the sediment. *Catena* 5(1): 1–8.

Appleby PG, Nolan PJ, Gifford DW et al. (1986) ^{210}Pb dating by low background gamma counting. *Hydrobiologia* 143(1): 21–27.

Arnell NW, Halliday SJ, Battarbee RW et al. (2015) The implications of climate change for the water environment in England. *Progress in Physical Geography* 39(1): 93–120.

Bahls LL (2013) *Encyonopsis from western North America: 31 species from Alberta, Idaho, Montana, Oregon, South Dakota, and Washington, including 17 species described as new. Northwest Diatoms*, vol. 5. Helena, MT: Montana Diatom Collection.

Bahls LL (2015) *Kurtkrammeria*, a new genus of freshwater diatoms (Bacillariophyta, Cymbellaceae) separated from *Encyonopsis*. *Nova Hedwigia* 101(1): 165–190.

Bannister W, McGowan S, Santos-Borja AC et al. (2019) Potential anthropogenic regime shifts in three freshwater lakes in Tropical East Asia. *Freshwater Biology* 64(4): 708–722.

Battarbee RW (1986) Diatom analysis. In: Berglund BE (ed) *Handbook of Holocene Palaeoecology and Palaeohydrology*. Chichester: John Wiley, pp. 527–570.

Battarbee RW (1999) The importance of palaeolimnology to lake restoration. *Hydrobiologia* 395: 149–159.

Battarbee RW and Kneen MJ (1982) The use of electronically counted microspheres in absolute diatom analysis. *Limnology and Oceanography* 27(1): 184–188.

Battarbee RW, Anderson NJ, Bennion H et al. (2012) Combining limnological and palaeolimnological data to disentangle the effects of nutrient pollution and climate change on lake ecosystems: Problems and potential. *Freshwater Biology* 57(10): 2091–2106.

Battarbee RW, Juggins S, Gasse F et al. (2000) European Diatom Database (EDDI). An information system for palaeoenvironmental reconstruction. In: *Proceedings of the European Climate Science Conference*, Vienna, 19–23 October 1998, pp. 1–10.

Battarbee RW, Turner S, Yang H et al. (2015) Air pollutant contamination and acidification of surface waters in the North York Moors, UK: Multi-proxy evidence from the sediments of a moorland pool. *The Holocene* 25(1): 226–237.

Benedict KB, Prenni AJ, Carrico CM et al. (2017) Enhanced concentrations of reactive nitrogen species in wildfire smoke. *Atmospheric Environment* 148: 8–15.

Bennett KD (1996) Determination of the number of zones in a biostratigraphical sequence. *The New Phytologist* 132(1): 155–170.

Bennion H, Carvalho L, Sayer CD et al. (2012) Identifying from recent sediment records the effects of nutrients and climate on diatom dynamics in Loch Leven. *Freshwater Biology* 57(10): 2015–2029.

Bennion H, Fluin J and Simpson GL (2004) Assessing eutrophication and reference conditions for Scottish freshwater lochs using subfossil diatoms. *Journal of Applied Ecology* 41(1): 124–138.

Bennion H, Simpson GL and Goldsmith BJ (2015) Assessing degradation and recovery pathways in lakes impacted by eutrophication using the sediment record. *Frontiers in Ecology and Evolution* 3: 94.

Bicudo DC, Tremarin PI, Almeida PD et al. (2016) Ecology and distribution of Aulacoseira species (Bacillariophyta) in tropical reservoirs from Brazil. *Diatom Research* 31(3): 199–215.

Bindler R, Renberg I and Brännvall ML (2001) A whole-basin study of sediment accumulation using stable lead isotopes and flyash particles in an acidified lake, Sweden. *Limnology and Oceanography* 46(1): 178–188.

Charles DF, Binford MW, Furlong ET et al. (1990) Paleoecological investigation of recent lake acidification in the Adirondack Mountains, NY. *Journal of Paleolimnology* 3(3): 195–241.

Chen M, Boyle EA, Switzer AD et al. (2016) A century long sedimentary record of anthropogenic lead (Pb), Pb isotopes and other trace metals in Singapore. *Environmental Pollution* 213: 446–459.

Chen Q and Taylor D (2018) Transboundary atmospheric pollution in Southeast Asia: Current methods, limitations and future developments. *Critical Reviews in Environmental Science and Technology* 48(16–18): 997–1029.

Curtis CJ and Simpson GL (2007) *Freshwater Umbrella – The Effects of Nitrogen Deposition & Climate Change on Freshwaters in the UK* (ECRC research report 115). London: Environmental Change Research Centre, University College London.

Dean WE (1974) Determination of carbonate and organic matter in calcareous sediments and sedimentary rocks by loss on ignition. *Journal of Sedimentary Petrology* 44(1): 242–248.

Donar CM, Neely RK and Stoermer EF (1996) Diatom succession in an urban reservoir system. *Journal of Paleolimnology* 15(3): 237–243.

Dong X, Sayer CD, Bennion H et al. (2008) Tracking eutrophication in Taihu Lake using the diatom record: Potential and problems. *Journal of Paleolimnology* 40(1): 413–429.

Dunnette PV, Higuera PE, McLauchlan KK et al. (2014) Biogeochemical impacts of wildfires over four millennia in a Rocky Mountain subalpine watershed. *The New Phytologist* 203(3): 900–912.

Energy Market Authority (2017) *Singapore Energy Statistics 2017*. Singapore: Energy Market Authority.

Engels S, Fong LSRZ, Chen Q et al. (2018) Historical atmospheric pollution trends in Southeast Asia inferred from lake sediment records. *Environmental Pollution* 235: 907–917.

Engstrom DR, Fitzgerald WF, Cooke CA et al. (2014) Atmospheric Hg emissions from preindustrial gold and silver extraction in the Americas: A reevaluation from lake-sediment archives. *Environmental Science and Technology* 48(12): 6533–6543.

Felix JD, Elliott EM and Shaw SL (2012) Nitrogen isotopic composition of coal-fired power plant NO_x: Influence of emission controls and implications for global emission inventories. *Environmental Science and Technology* 46(6): 3528–3535.

Fontana L, Albuquerque ALS, Brenner M et al. (2014) The eutrophication history of a tropical water supply reservoir in Brazil. *Journal of Paleolimnology* 51(1): 29–43.

Grimm EC (1987) CONISS: A FORTRAN 77 program for stratigraphically constrained cluster analysis by the method of incremental sum of squares. *Computers & Geosciences* 13(1): 13–35.

Gworek B, Dmuchowski W, Baczewska AH et al. (2017) Air contamination by mercury, emissions and transformations – A review. *Water, Air, and Soil Pollution* 228(4): 123.

Hastings MG, Jarvis JC and Steig EJ (2009) Anthropogenic impacts on nitrogen isotopes of ice-core nitrate. *Science* 324(5932): 1288.

Hobæk A, Løvik JE, Rohrlack T et al. (2012) Eutrophication, recovery and temperature in Lake Mjøsa: Detecting trends with monitoring data and sediment records. *Freshwater Biology* 57(10): 1998–2014.

Jones VJ, Battarbee RW, Rose NL et al. (1997) Evidence for the pollution of Loch Ness from the analysis of its recent sediments. *Science of the Total Environment* 203(1): 37–49.

Jones VJ, Rose NL, Self AE et al. (2014) Evidence of global pollution and recent environmental change in Kamchatka, Russia. *Global and Planetary Change* 134: 82–90.

Juggins S (2013) Quantitative reconstructions in palaeolimnology: New paradigm or sick science? *Quaternary Science Reviews* 64: 20–32.

Juggins S and Birks HJB (2012) Quantitative environmental reconstructions from biological data. In: Birks HJB, Lotter AF, Juggins S et al. (eds) *Tracking Environmental Change Using Lake Sediments: Data Handling and Numerical Techniques*, vol. 5. Dordrecht: Springer, pp. 431–494.

Karthik KRG, Baikie T, Mohan Dass ET et al. (2017) Understanding the Southeast Asian haze. *Environmental Research Letters* 12(8): 84018.

Kimmel BL and Groeger AW (1986) Limnological and ecological changes associated with reservoir aging. In: Hall GE and van den Avyle MJ (eds) *Reservoir Fisheries Management: Strategies for the 80s*. Bethesda: American Fisheries Society, pp. 327.

Koplitz SN, Jacob DJ, Sulprizio MP et al. (2017) Burden of disease from rising coal-fired power plant emissions in Southeast Asia. *Environmental Science and Technology* 51(3): 1467–1476.

Korhola A, Sorvari S, Rautio M et al. (2002) A multi-proxy analysis of climate impacts on the recent development of subarctic Lake Saanajärvi in Finnish Lapland. *Journal of Paleolimnology* 28(1): 59–77.

Köster D, Racca JMJ and Pienitz R (2004) Diatom-based inference models and reconstructions revisited: Methods and transformations. *Journal of Paleolimnology* 32(3): 233–245.

Krammer K (2000) *Diatoms of Europe: Diatoms of the European Inland Waters and Comparable Habitats: The Genus Pinnularia*, vol. 1. Ruggell: ARG Gantner Verlag KG.

Krammer K and Lange-Bertalot H (1986) *Bacillariophyceae. 1. Teil: Naviculaceae. Band 2/1*. Stuttgart: Gustav Fisher Verlag.

Krammer K and Lange-Bertalot H (1988) *Bacillariophyceae. 2. Teil: Bacillariaceae, Epithemiaceae, Surirellaceae. Band 2/2*. Berlin: Spektrum Akademischer Verlag.

Krammer K and Lange-Bertalot H (1991a) *Bacillariophyceae. 3. Teil: Centrales, Fragilariaceae, Eunotiaceae. Band 2/3*. Stuttgart: Gustav Fisher Verlag.

Krammer K and Lange-Bertalot H (1991b) *Bacillariophyceae. 4. Teil: Achnanthaceae, kritsche ergänzungen zu Navicula (Lineolatae) und Gomphonema Gesamliteraturverzeichnis. Band 2/4*. Stuttgart: Gustav Fisher Verlag.

Lange-Bertalot H and Moser G (1994) *BRACHYSIRA Monographie der Gattung. Band 29*. Berlin: J Cramer.

Lange-Bertalot H, Bąk M, Witkowski A et al. (2011) *Diatoms of Europe. Diatoms of the European Inland Waters and Comparable Habitats: Eunotia and Some Related Genera*, vol. 6. Ruggell: ARG Gantner Verlag KG.

Lange-Bertalot H, Hofmann G, Werum M et al. (2017) *Freshwater Benthic Diatoms of Central Europe: Over 800 Common Species Used in Ecological Assessment*. Schmitten-Oberreifenberg: Koeltz Botanical Books.

Lasko K, Vadrevu KP and Nguyen TTN (2018) Analysis of air pollution over Hanoi, Vietnam using multi-satellite and MERRA reanalysis datasets. *PLoS ONE* 13(5): 1–21.

Last WM and Smol JP (2001) An introduction to basin analysis, coring, and chronological techniques used in paleolimnology. In: Last WM and Smol JP (eds) *Tracking Environmental Change Using Lake Sediments. Volume 1: Basin Analysis, Coring, and Chronological Techniques*. Dordrecht: Kluwer Academic Publishers, pp. 1–5.

Lau GN (1988) The power house – 25 years of development in electricity generation in Singapore. *PUB Digest* 9: 34–41.

Lee JSH, Jaafar Z, Tan AKJ et al. (2016) Toward clearer skies: Challenges in regulating transboundary haze in Southeast Asia. *Environmental Science and Policy* 55: 87–95.

Leng MJ, Lamb AL, Heaton THE et al. (2006) Isotopes in lake sediments. In: Leng MJ (ed) *Isotopes in Palaeoenvironmental Research*. Dordrecht: Springer, pp. 147–184.

Lewis WM Jr (1996) Tropical lakes: How latitude makes a difference. In: Schiemer F and Boland KT (eds) *Perspectives in Tropical Limnology*. Amsterdam: SPB Academic Publishers, pp. 43–64.

Low EW and Ng PKL (2010) Top-down control of phytoplankton by zooplankton in tropical reservoirs in Singapore? *Raffles Bulletin of Zoology* 58(2): 311–322.

MacDonald DD, Ingersoll CG and Berger TA (2000) Development and evaluation of consensus-based sediment quality guidelines for freshwater ecosystems. *Archives of Environmental Contamination and Toxicology* 39(1): 20–31.

Marsicano LJ, Hartranft JL, Siver PA et al. (1995) An historical account of water quality changes in Candlewood Lake, Connecticut, over a sixty year period using paleolimnology and ten years of monitoring data. *Lake and Reservoir Management* 11(1): 15–28.

Meyers PA (1994) Preservation of elemental and isotopic source identification of sedimentary organic matter. *Chemical Geology* 114(3): 289–302.

Meyers PA (2003) Applications of organic geochemistry to paleolimnological reconstructions: A summary of examples from the Laurentian Great Lakes. *Organic Geochemistry* 34(2): 261–289.

Mills K, Schillereff D, Saulnier-Talbot É et al. (2017) Deciphering long-term records of natural variability and human impact as recorded in lake sediments: A palaeolimnological puzzle. *Water* 4(2): e1195.

Ministry of Defence (1978) Singapore topographic map. Available at: http://www.nas.gov.sg/archivesonline/maps_building _plans/record-details/faf72be6-115c-11e3-83d5-0050568939ad (accessed 28 November 2018).

Nagafuchi O, Rose NL, Hoshika A et al. (2009) The temporal record and sources of atmospherically deposited fly-ash particles in Lake Akagikonuma, a Japanese mountain lake. *Journal of Paleolimnology* 42(3): 359–371.

Ng MP and Lung YW (1985) The use of electrostatic precipitators at Senoko Power Station. *PUB Digest* 3: 16–23.

OECD (1982) *Eutrophication of Waters: Monitoring, Assessment and Control*. Paris: OECD.

OpenStreetMap Contributors (2018) OpenStreetMap. Available at: https://www.openstreetmap.org/#map=12/1.3625/103.8392 (accessed 26 November 2018).

Pacyna JM, Travnikov O, de Simone F et al. (2016) Current and future levels of mercury atmospheric pollution on a global scale. *Atmospheric Chemistry and Physics* 16(19): 12495–12511.

Page SE, Hoscilo A, Langner A et al. (2009) Tropical peatland fires in Southeast Asia. In: Cochrane MA (ed) *Tropical Fire Ecology: Climate Change, Land Use, and Ecosystem Dynamics*. Berlin: Springer, pp. 263–287.

Pla S, Monteith D, Flower R et al. (2009) The recent palaeolimnology of a remote Scottish loch with special reference to the relative impacts of regional warming and atmospheric contamination. *Freshwater Biology* 54(3): 505–523.

R Core Team (2018) R: A language and environment for statistical computing. Vienna: Foundation for Statistical Computing.

Reinemann SA, Porinchu DF, Gustin MS et al. (2014) Historical trends of mercury and spheroidal carbonaceous particle deposition in sub-alpine lakes in the Great Basin, United States. *Journal of Paleolimnology* 52(4): 405–418.

Renberg I (1990) A procedure for preparing large sets of diatom slides from sediment cores. *Journal of Paleolimnology* 4(1): 87–90.

Rose NL (1994) A note on further refinements to a procedure for the extraction of carbonaceous fly-ash particles from sediments. *Journal of Paleolimnology* 11(2): 201–204.

Rose NL (2001) Fly-ash particles. In: Last WM and Smol JP (eds) *Tracking Environmental Change Using Lake Sediments. Vol. 2: Physical and Geochemical Methods*. Dordrecht: Kluwer Academic Publishers, pp. 319–349.

Rose NL (2008) Quality control in the analysis of lake sediments for spheroidal carbonaceous particles. *Limnology and Oceanography: Methods* 6(4): 172–179.

Rose NL (2015) Spheroidal carbonaceous fly ash particles provide a globally synchronous stratigraphic marker for the Anthropocene. *Environmental Science and Technology* 49(7): 4155–4162.

Rose NL and Appleby PG (2005) Regional applications of lake sediment dating by spheroidal carbonaceous particle analysis I: United Kingdom. *Journal of Paleolimnology* 34(3): 349–361.

Rose NL, Boyle JF, Du Y et al. (2004) Sedimentary evidence for changes in the pollution status of Taihu in the Jiangsu region of eastern China. *Journal of Paleolimnology* 32(1): 41–51.

Rose NL, Harlock S and Appleby PG (1999) Within-basin profile variability and cross-correlation of lake sediment cores using the spheroidal carbonaceous particle record. *Journal of Paleolimnology* 21(1): 85–96.

Rudnick RL and Gao S (2013) Composition of the continental crust. *Treatise on Geochemistry* 3: 1–64.

Rühland KM and Smol JP (2005) Diatom shifts as evidence for recent Subarctic warming in a remote tundra lake, NWT, Canada. *Palaeogeography, Palaeoclimatology, Palaeoecology* 226(1): 1–16.

Rühland KM, Paterson AM and Smol JP (2015) Lake diatom responses to warming: Reviewing the evidence. *Journal of Paleolimnology* 54(1): 1–35.

Ryves DB, Juggins S, Fritz SC et al. (2006) Physical and chemical predictors of diatom dissolution in freshwater and saline lake sediments in North America. *Limnology and Oceanography* 51(3): 1355–1368.

Saros JE and Anderson NJ (2015) The ecology of the planktonic diatom. Cyclotella and its implications for global environmental change studies. *Biological Reviews* 90(2): 522–541.

Saulnier-Talbot É (2016) Paleolimnology as a tool to achieve environmental sustainability in the Anthropocene: An overview. *Geosciences* 6(2): 26.

Singapore Land Authority (1945) Malaya – Singapore and Johore Bahru. Available at: http://www.nas.gov.sg/archivesonline /maps_building_plans/record-details/fb73a558-115c-11e3 -83d5-0050568939ad (accessed 23 November 2018)

Singapore National Environment Agency (2009) *Guidebook on the Climate of Singapore*. Singapore: Singapore National Environment Agency.

Smol JP (2010) The power of the past: Using sediments to track the effects of multiple stressors on lake ecosystems. *Freshwater Biology* 55: 43–59.

Smol JP and Stoermer EF (eds) (2010) *The Diatoms: Applications for the Environmental and Earth Sciences*. Cambridge: Cambridge University Press.

Steffen W, Broadgate W, Deutsch L et al. (2015) The trajectory of the Anthropocene: The Great Acceleration. *The Anthropocene Review* 2(1): 81–98.

Sundarambal P, Tkalich P, Balasubramanian R et al. (2010) Impact of biomass burning on ocean water quality in Southeast Asia through atmospheric deposition: Field observations. *Atmospheric Chemistry and Physics* 10(23): 11323–11336.

Swain EB, Jakus PM, Rice G et al. (2007) Socioeconomic consequences of mercury use and pollution. *Ambio* 36(1): 45–61.

Talling JF and Lemoalle J (1998) *Ecological Dynamics of Tropical Inland Waters*. Cambridge: Cambridge University Press.

The National Archives UK (1915) Map of the island of Singapore and its dependencies. Available at: http://www.nas.gov.sg /archivesonline/maps_building_plans/record-details/b57a2906 -57a3-11e6-b4c5-0050568939ad (accessed 28 November 2018)

Tortajada C, Joshi YK and Biswas AK (2013) *The Singapore Water Story: Sustainable Development in an Urban City State*. New York: Routledge.

United Nations Environment Programme (2019) *Global Mercury Assessment 2018*. Geneva: United Nations Environment Programme.

United Nations Population Division (2018) *World Urbanization Prospects: The 2018 Revision*. New York: United Nations.

Urban Redevelopment Authority (2014) URA Master Plan 2014. Available at: https://www.ura.gov.sg/maps/ (accessed 26 November 2018).

U.S. Energy Information Administration (2016) International Energy Statistics. Available at: https://www.eia.gov/beta/international/data/browser/ (accessed 17 November 2018).

van Dam H, Sinkeldam JA and Mertens A (1994) A coded check list and ecological indicator values of freshwater diatoms from the Netherlands. *Aquatic Ecology* 28(1): 117–133.

Wang YL, Liu XY, Song W et al. (2017) Source appointment of nitrogen in PM2.5 based on bulk $\delta^{15}N$ signatures and a Bayesian isotope mixing model. *Tellus, Series B: Chemical and Physical Meteorology* 69(1): 1–10.

Warnford-Lock CG (1907) *Mining in Malaya for Gold and Tin*. London: Crowther and Goodman.

Wengrat S, Padial AA, Jeppesen E et al. (2018) Paleolimnological records reveal biotic homogenization driven by eutrophication in tropical reservoirs. *Journal of Paleolimnology* 60: 299–309.

Wiltse B, Paterson AM, Findlay DL et al. (2016) Seasonal and decadal patterns in *Discostella* (Bacillariophyceae) species from bi-weekly records of two boreal lakes (Experimental Lakes Area, Ontario, Canada). *Journal of Phycology* 52(5): 817–826.

Wong TC and Yap ALH (2004) *Four Decades of Transformation: Land Use in Singapore, 1960–2000*. Singapore: Eastern Universities Press.

Wong YK, Chew PT and Ibrahim AB (1994) The tree communities of the Central Catchment Nature Reserve, Singapore. *Gardens' Bulletin Singapore* 46: 37–78.

World Bank (1989) *World Development Report 1989: Financial Systems and Development, World Development Report*. New York: World Bank.

Yan Y, Wang L, Li J et al. (2018) Diatom response to climatic warming over the last 200 years: A record from Gonghai Lake, North China. *Palaeogeography, Palaeoclimatology, Palaeoecology* 495: 48–59.

Yang H and Rose NL (2003) Distribution of mercury in six lake sediment cores across the UK. *Science of the Total Environment* 304(1): 391–404.

Yang H, Turner S and Rose NL (2016) Mercury pollution in the lake sediments and catchment soils of anthropogenically-disturbed sites across England. *Environmental Pollution* 219: 1092–1101.

Yang SL and Chiam-Tai YC (1991) Algae and algal blooms in Singapore reservoirs. *PUB R&D Journal* 3: 17–27.

Yeo DCJ and Lim KKP (2011) Freshwater ecosystems. In: Ng PKL, Corlett RT and Tan HTW (eds) *Singapore Biodiversity: An Encyclopedia of the Natural Environment and Sustainable Development*. Singapore: Editions Didier Millet in association with the Raffles Museum of Biodiversity Research, pp. 52–64.

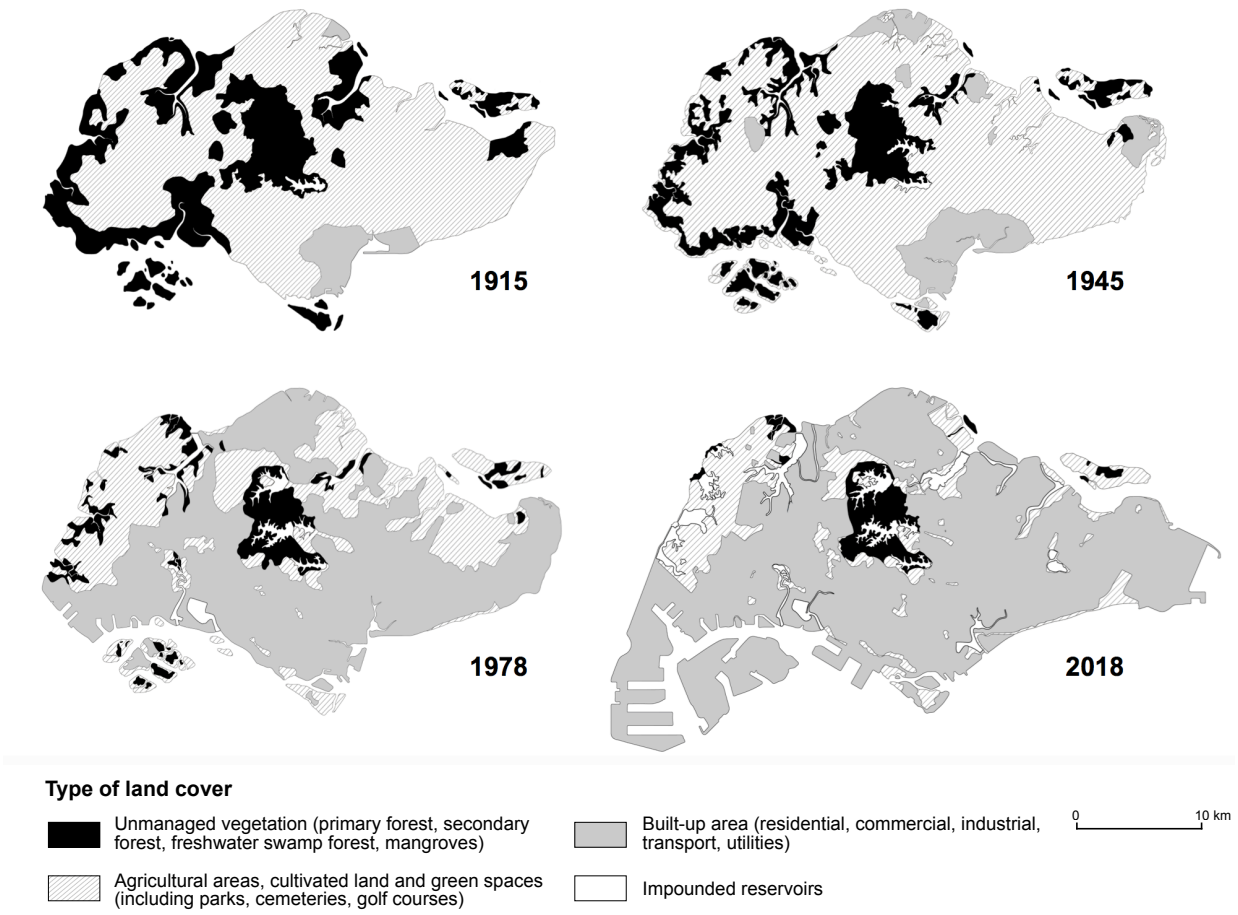

Figure 1. 100 years of land cover change in Singapore. The maps were created based on four classifications of land cover types: (i) unmanaged vegetation, (ii) agricultural areas, cultivated land, and other green spaces, (iii) built-up areas, and (iv) impounded reservoirs. The AD 1915 map was adapted from The National Archives UK (1915), the AD 1945 map adapted from the Singapore Land Authority (1945), the AD 1978 map adapted from the Ministry of Defence (1978), and the AD 2018 map adapted from the Urban Redevelopment Authority (2014) and OpenStreetMap (2018).

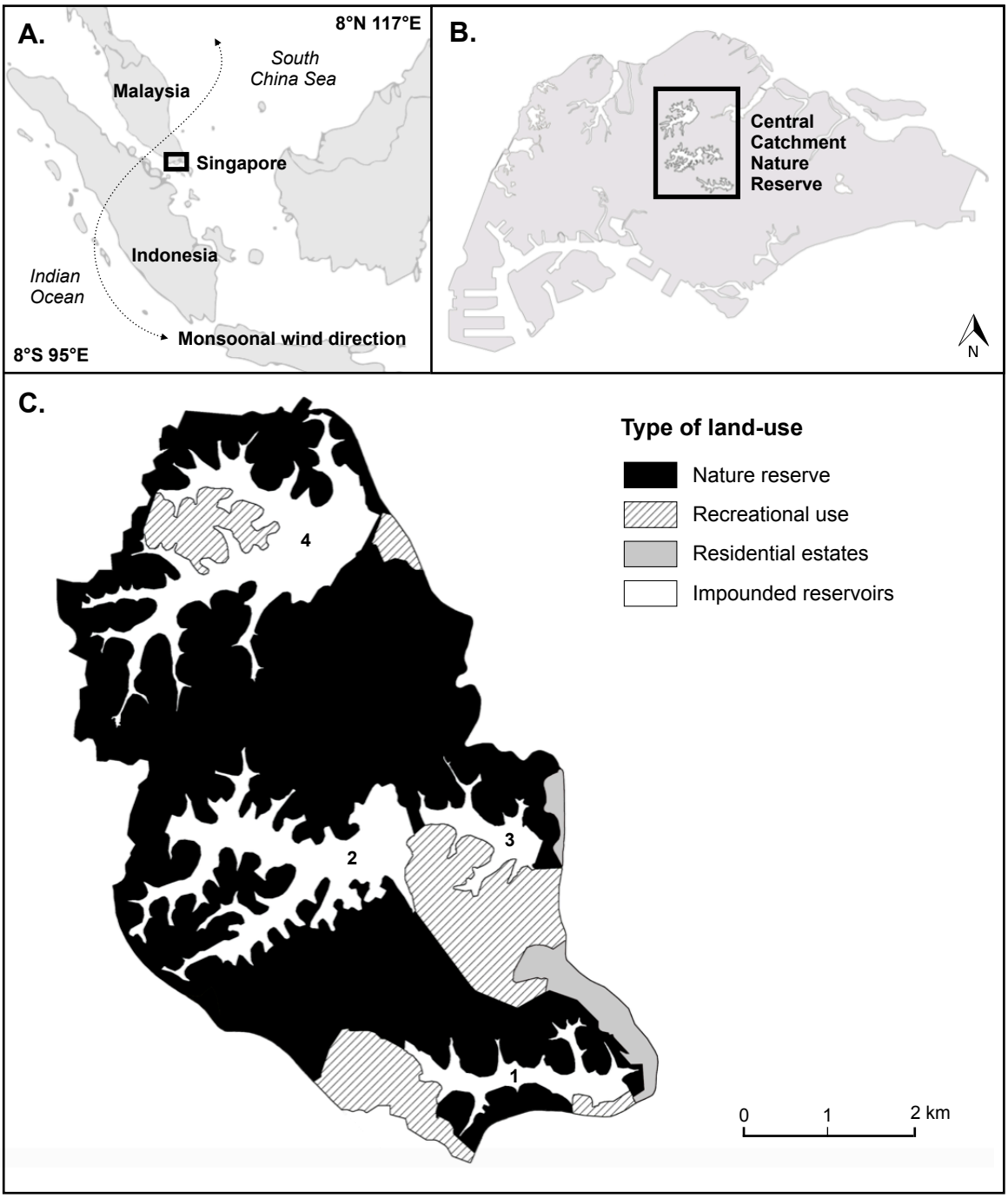

Figure 2. Geographical location of the study site. **A.** Map of Singapore and its neighbouring countries, Malaysia and Indonesia, along with the general wind flow patterns in the region during the northeast and southwest monsoons. **B.** Relative position of the Central Catchment Nature Reserve on the mainland of Singapore. **C.** Land-use and catchment map of the Central Catchment Nature Reserve.

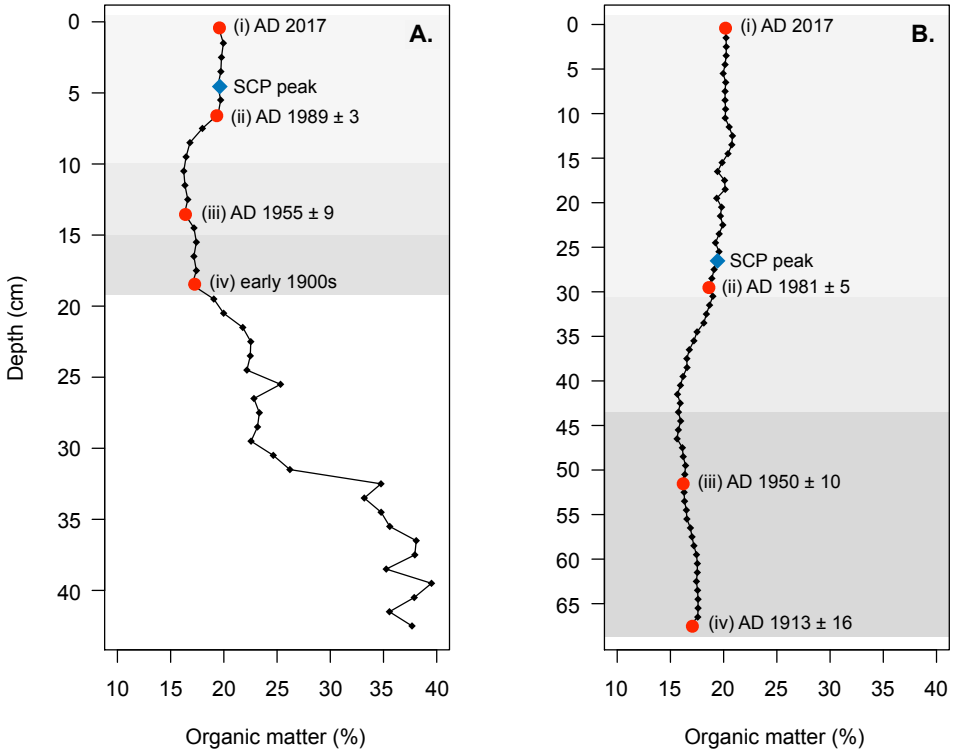

Figure 3. Core correlation between MRR1 and MRR2. Down-core variations in organic matter content (%LOI) for **A.** MRR1 (0–43 cm) and **B.** MRR2 (0–68 cm). Points (i)–(iv) are where both cores exhibit similar magnitudes of and changes in organic matter and are therefore likely to correspond to the same time period. The depths at which SCP depositions peak in both cores are shown. The shaded areas represent corresponding diatom assemblage zones.

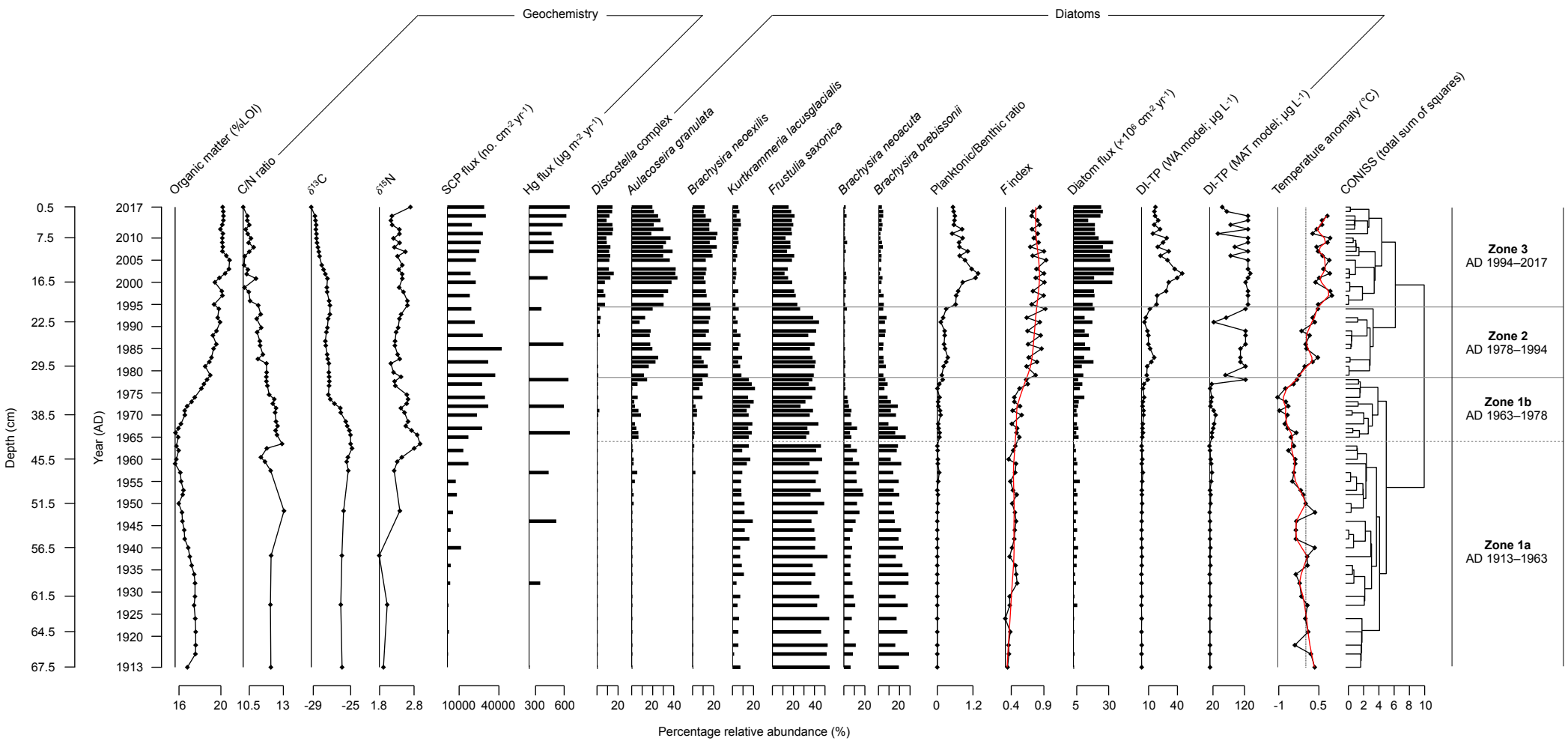

Figure 4. Composite summary diagram showing the sedimentary record for MRR2 plotted against the ^{210}Pb-derived calendar dates and core depth. Data include organic matter content (%LOI), atomic C/N ratios, carbon and nitrogen stable isotopes ($\delta^{13}C$ and $\delta^{15}N$), spheroidal carbonaceous particle accumulation rates (SCP flux), mercury accumulation rates (Hg flux), selected diatom taxa, the ratio of planktonic to benthic diatoms, the diatom preservation index (*F* index), diatom accumulation rates (diatom flux), diatom-inferred total phosphorus values derived from the weighted-averaging model and the modern analogue technique, and historical mean annual surface air temperature anomalies. Diatoms have been ordered according to their ascending weighted average abundance in the core. The diatom stratigraphy is also numerically zoned according to the clusters identified in the dendrogram.

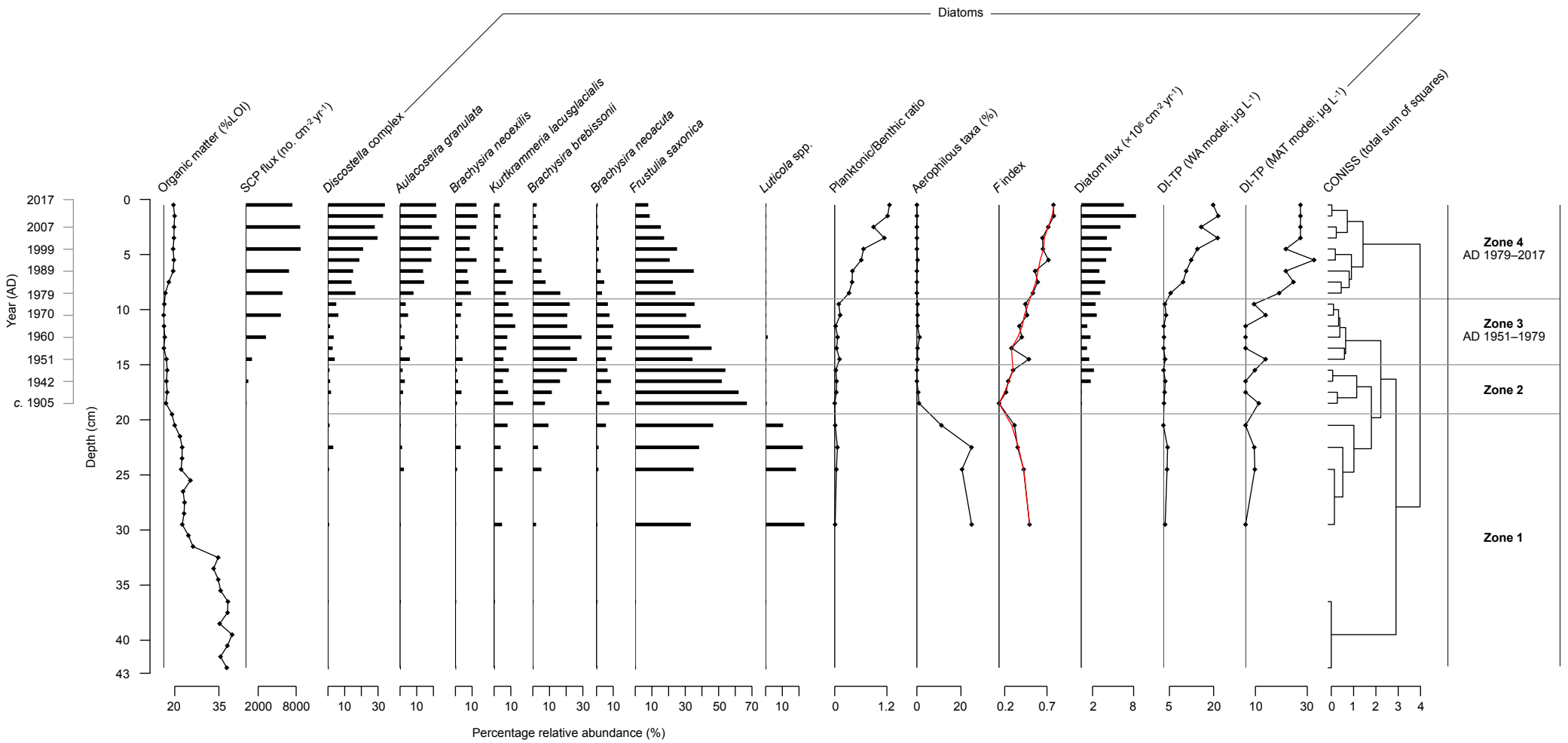

Figure 5. Composite summary diagram showing the sedimentary record for MRR1 plotted against core depth and the ^{210}Pb-derived calendar dates. Data include organic matter content (%LOI), spheroidal carbonaceous particle accumulation rates (SCP flux), selected diatom taxa, the ratio of planktonic to benthic diatoms, the proportion of aerophilous taxa, the diatom preservation index (*F* index), diatom accumulation rates (diatom flux), and diatom-inferred total phosphorus values derived from the weighted-averaging model and the modern analogue technique. Diatoms have been ordered according to their ascending weighted average abundance in the core. The diatom stratigraphy is also numerically zoned according to the clusters identified in the dendrogram.

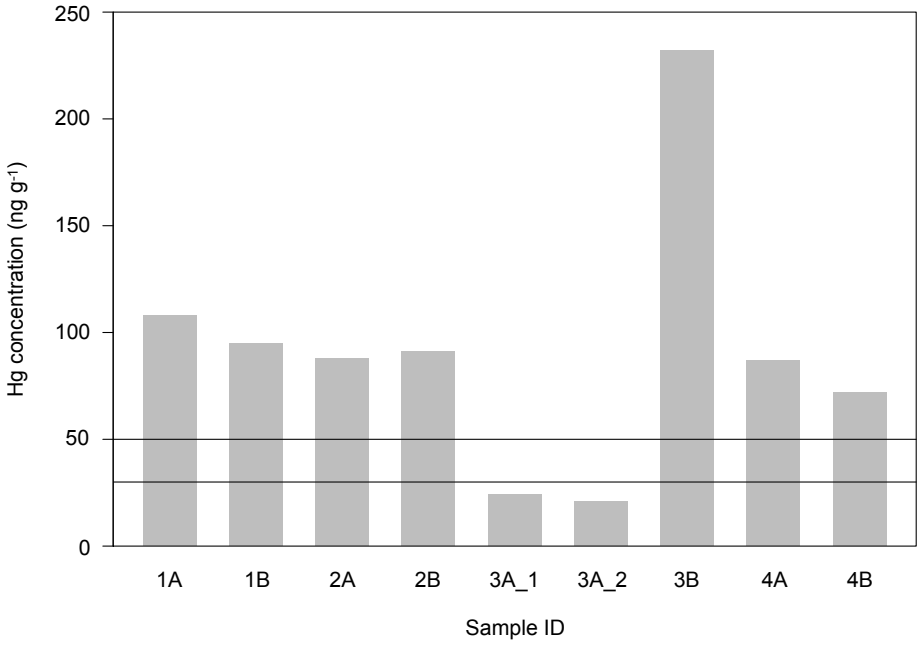

Figure 6. Deep soil Hg concentrations from the forested catchment soils of the study site. The horizontal line at 30 ng g^{-1} represents Hg levels typically associated with soils situated on a bedrock geology comprising granite (Yang and Rose, 2003) while the line at 50 ng g^{-1} represents the average concentration of Hg in Earth's upper continental crust (Rudnick and Gao, 2013). Sample 3A was processed twice to confirm the low concentrations.

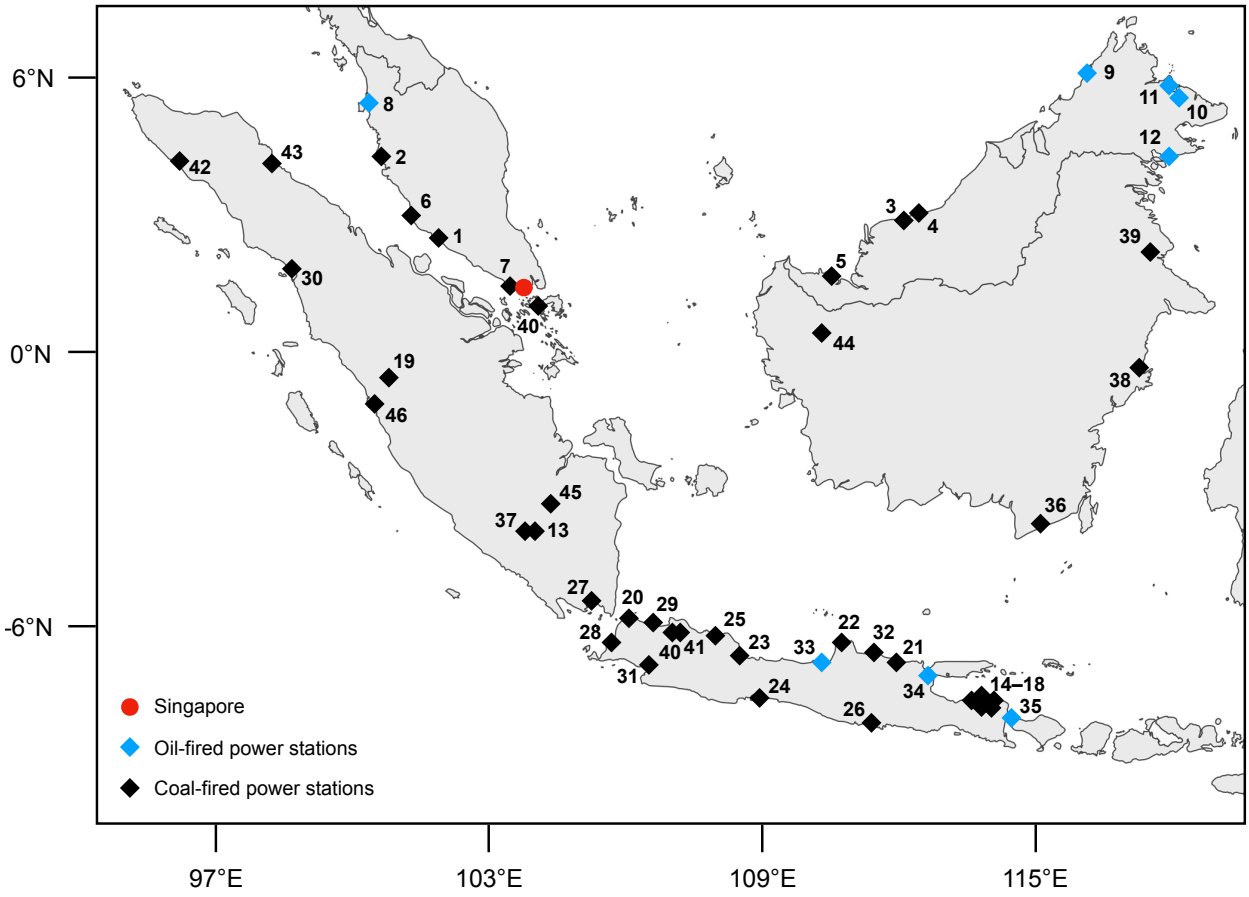

Figure 7. Map of all operating coal and oil-fired power stations in Malaysia and in Indonesia (Sumatra, Java and Kalimantan). The details of each power station are provided in Supplementary Table 4.

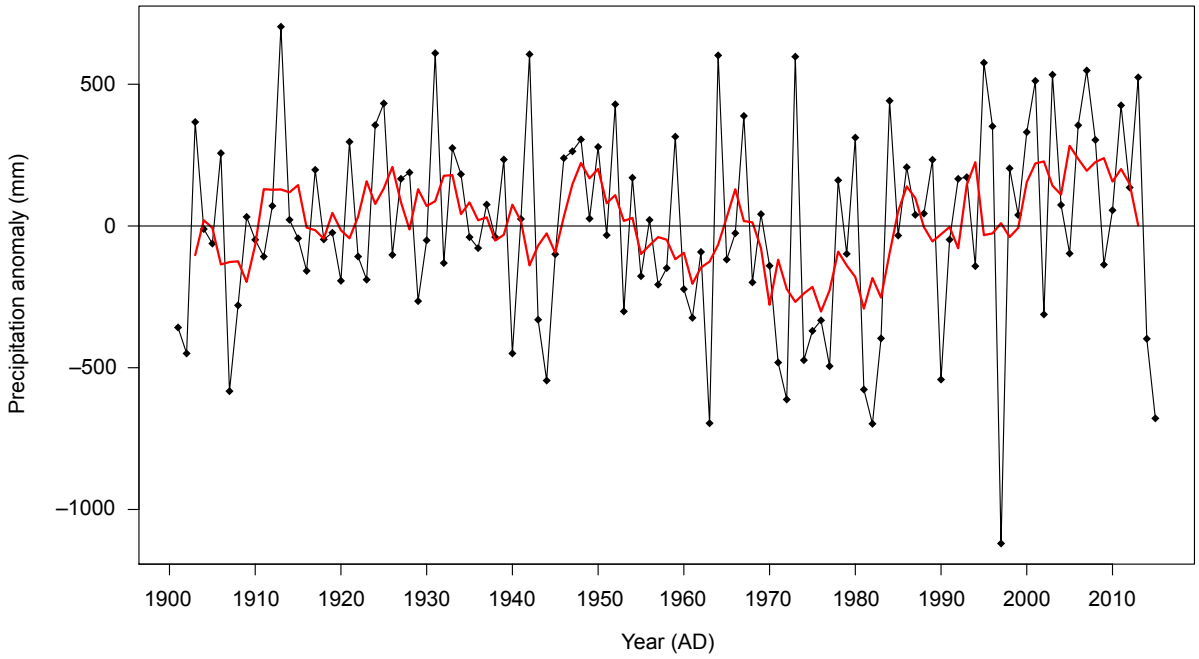

Supplementary Figure 1. Annual total precipitation deviations from the long-term mean over AD 1901–2015 in Singapore. A 5-year smoother is plotted using moving averages of the precipitation anomalies.

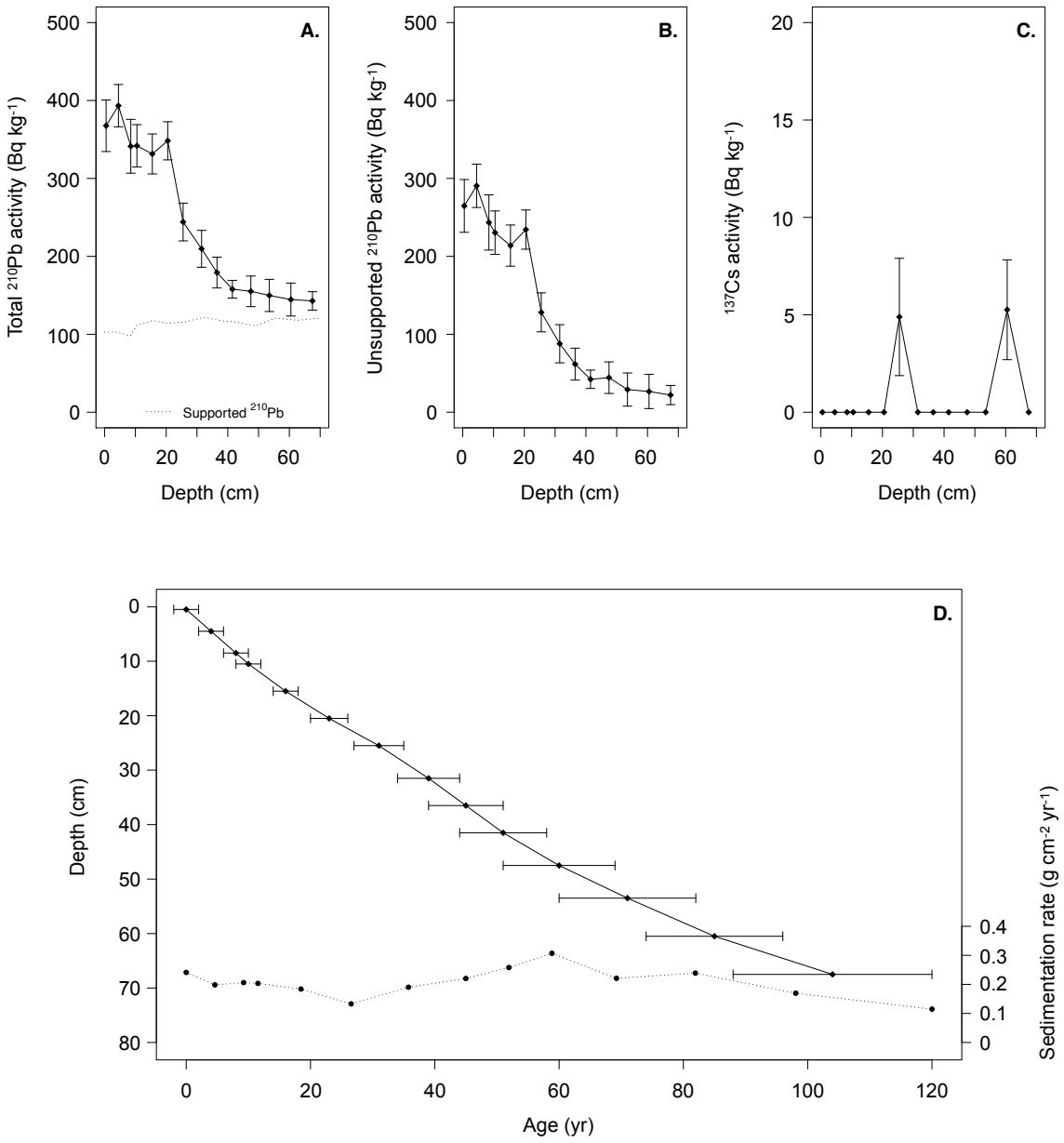

Supplementary Figure 2. ^{210}Pb and ^{137}Cs data for MRR2. **A.** Total and supported ^{210}Pb activities. **B.** Unsupported ^{210}Pb activities. **C.** ^{137}Cs activity profile. **D.** ^{210}Pb chronology and dry mass sediment accumulation rates. Linear interpolation with weighted averaging between the dated horizons was used to assign calendar dates and sediment accumulation rates to the remaining samples.

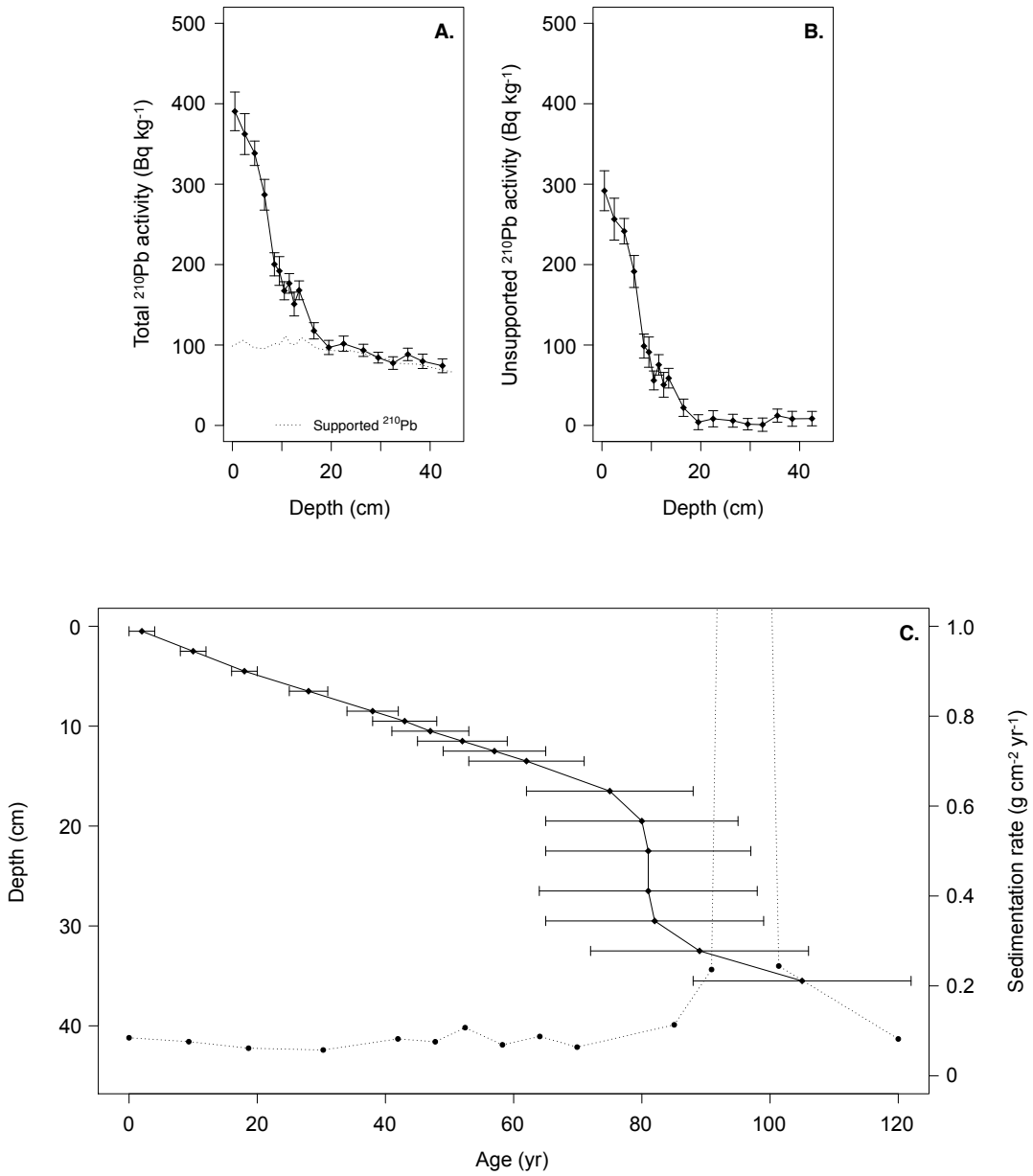

Supplementary Figure 3. ^{210}Pb data for MRR1. **A.** Total and supported ^{210}Pb activities. **B.** Unsupported ^{210}Pb activities. **C.** ^{137}Cs activity profile. **D.** ^{210}Pb chronology and dry mass sediment accumulation rates. Linear interpolation with weighted averaging between the dated horizons was used to assign calendar dates and sediment accumulation rates to the remaining samples. No ^{137}Cs activity was detected in the analysed samples.

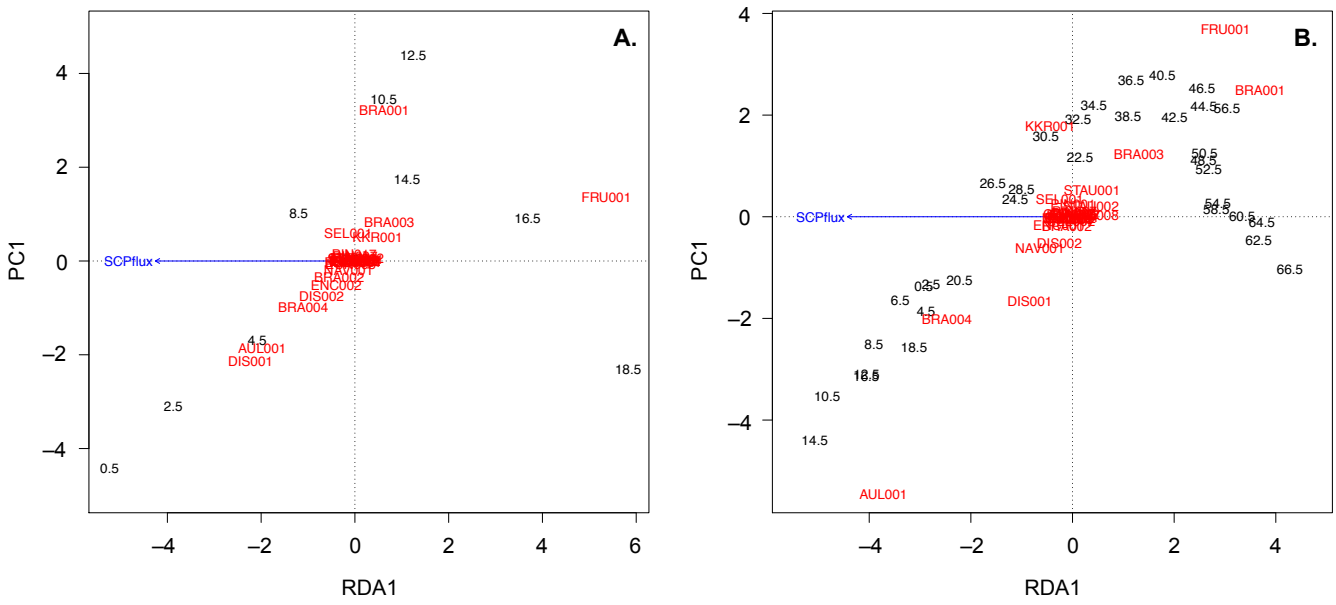

Supplementary Figure 4. Redundancy analysis (RDA) biplots for **A.** MRR1 and **B.** MRR2. Each arrow represents the approximate (linear) correlation coefficient between diatoms and SCP fluxes. Diatom species are given as codes; corresponding taxonomic names can be found in Supplementary Table 3.

Supplementary Table 1a. ^{210}Pb concentrations for MRR2.

Depth	Dry mass	^{210}Pb					
		Total		Supported		Unsupported	
cm	g cm^{-2}	Bq kg^{-1}	±	Bq kg^{-1}	±	Bq kg^{-1}	±
0.5	0.06	367.61	33.06	102.86	7.28	264.75	33.85
4.5	0.78	393.38	27.13	102.86	5.97	290.52	27.78
8.5	1.68	341.28	34.52	97.79	7.79	243.49	35.39
10.5	2.13	341.85	27.17	111.43	6.26	230.42	27.88
15.5	3.22	331.44	25.62	117.62	6.41	213.82	26.41
20.5	4.39	348.3	24.48	113.95	5.76	234.35	25.15
25.5	5.63	244.11	24.22	115.94	6.10	128.17	24.98
31.5	7.14	209.69	23.68	121.84	6.22	87.85	24.48
36.5	8.63	179.23	19.78	117.52	5.22	61.71	20.46
41.5	10.46	157.87	11.33	115.58	3.11	42.29	11.75
47.5	12.83	155.15	19.61	110.8	5.10	44.35	20.26
53.5	15.35	149.85	20.6	120.73	5.38	29.12	21.29
60.5	18.16	144.62	21.16	118.01	5.78	26.61	21.94
67.5	20.79	142.85	11.81	120.8	3.47	22.05	12.31

Supplementary Table 1b. ^{137}Cs concentrations for MRR2.

Depth	^{137}Cs	
cm	Bq kg^{-1}	±
0.5	0	0
4.5	0	0
8.5	0	0
10.5	0	0
15.5	0	0
20.5	0	0
25.5	4.89	3.01
31.5	0	0
36.5	0	0
41.5	0	0
47.5	0	0
53.5	0	0
60.5	5.26	2.56
67.5	0	0

Supplementary Table 1c. ^{210}Pb chronology for MRR2.

Depth	Dry mass	Chronology			Sedimentation Rate		
		Year	Age				
cm	g cm^{-2}	AD	yr	±	g cm^{-2} yr^{-1}	cm yr^{-1}	±%
0	0	2017	0				
0.5	0.06	2017	0	2	0.2412	1.391	14.5
4.5	0.78	2013	4	2	0.1984	0.98	12.1
8.5	1.68	2009	8	2	0.2061	0.918	16.8
10.5	2.13	2007	10	2	0.2034	0.926	15
15.5	3.22	2001	16	2	0.184	0.813	16
20.5	4.39	1994	23	3	0.1329	0.552	16.5
25.5	5.63	1986	31	4	0.1903	0.761	24.7
31.5	7.14	1978	39	5	0.2203	0.806	33.3
36.5	8.63	1972	45	6	0.2579	0.776	39.3
41.5	10.46	1966	51	7	0.3071	0.804	37.5
47.5	12.83	1957	60	9	0.2208	0.542	54.4
53.5	15.35	1946	71	11	0.2388	0.583	80.2
60.5	18.16	1932	85	11	0.1697	0.437	88.2
67.5	20.79	1913	104	16	0.1148	0.304	74.8

Supplementary Table 2a. ^{210}Pb concentrations for MRR1.

Depth	Dry mass	^{210}Pb					
		Total		Supported		Unsupported	
cm	g cm^{-2}	Bq kg^{-1}	±	Bq kg^{-1}	±	Bq kg^{-1}	±
0.5	0.16	390.52	24.03	98.71	6.26	291.81	24.83
2.5	0.77	362.26	25.4	105.76	5.66	256.5	26.02
4.5	1.37	338.4	15.19	96.87	4.3	241.53	15.79
6.5	1.94	286.84	19.09	95.42	5.58	191.42	19.89
8.5	2.61	200.33	14.39	101.65	4.18	98.68	14.98
9.5	3.01	192.02	17.87	100.87	5.89	91.15	18.82
10.5	3.42	167.45	11.26	111.52	3.36	55.93	11.75
11.5	3.81	176.61	12.17	101.27	3.49	75.34	12.66
12.5	4.21	150.94	14.8	100.41	4.12	50.53	15.36
13.5	4.61	167.98	11.72	109.25	3.44	58.73	12.21
16.5	5.68	117.65	10.12	95.64	3.64	22.01	10.75
19.5	6.82	96.96	8.8	92.93	3.03	4.03	9.31
22.5	8.16	101.6	9.49	93.32	3.29	8.28	10.04
26.5	10.28	93.37	7.57	87.52	2.63	5.85	8.01
29.5	12.11	84.29	6.71	82.76	2.36	1.53	7.11
32.5	13.84	77.54	7.82	76.6	2.7	0.94	8.27
35.5	15.06	88.34	7.73	76.18	2.66	12.16	8.17
38.5	15.99	79.75	8.95	71.51	2.48	8.24	9.29
42.5	17.23	74.17	8.6	65.68	2.54	8.49	8.97

Supplementary Table 2b. ^{137}Cs concentrations for MRR1.

Depth	^{137}Cs	
cm	Bq kg^{-1}	±
0.5	0	0
2.5	0	0
4.5	0	0
6.5	0	0
8.5	0	0
9.5	0	0
10.5	0	0
11.5	0	0
12.5	0	0
13.5	0	0
16.5	0	0
19.5	0	0
22.5	0	0
26.5	0	0
29.5	0	0
32.5	0	0
35.5	0	0
38.5	0	0
42.5	0	0

Supplementary Table 2c. ^{210}Pb chronology for MRR1.

Depth	Dry mass	Chronology			Sedimentation Rate		
		Year	Age				
cm	g cm^{-2}	AD	yr	±	g cm^{-2} yr^{-1}	cm yr^{-1}	±%
0	0	2017	0				
0.5	0.16	2015	2	2	0.0846	0.274	8.4
2.5	0.77	2007	10	2	0.0759	0.25	10.1
4.5	1.37	1999	18	2	0.0614	0.21	11.2
6.5	1.94	1989	28	3	0.0574	0.186	15.6
8.5	2.61	1979	38	4	0.0821	0.23	21.6
9.5	3.01	1974	43	5	0.0757	0.187	27.2
10.5	3.42	1970	47	6	0.1071	0.267	29.2
11.5	3.81	1965	52	7	0.0689	0.174	28.7
12.5	4.21	1960	57	8	0.0875	0.221	40.6
13.5	4.61	1955	62	9	0.0638	0.174	37.4
16.5	5.68	1942	75	13	0.1134	0.307	65.6
19.5	6.82	1937	80	15	0.2364	0.572	87.2
22.5	8.16	1936	81	16	1.3345	2.703	113.3
26.5	10.28	1936	81	17	14.5819	25.798	158
29.5	12.11	1935	82	17	6.2782	10.565	194.9
32.5	13.84	1928	89	17	0.2442	0.497	230.3
35.5	15.06	1912	105	17	0.082	0.229	78.5

Supplementary Table 3. List of all diatom species and their authorities identified in this study. Species codes are specific to this research.

Code	Species Name	Authority
AUL001	*Aulacoseira granulata*	(Ehrenberg) Simonsen
BRA001	*Brachysira brebissonii*	R. Ross
BRA002	*Brachysira vitrea*	(Grunow) R. Ross
BRA003	*Brachysira neoacuta*	Lange-Bertalot
BRA004	*Brachysira neoexilis*	Lange-Bertalot
CAL001	*Caloneis* sp.1	
CRA002	*Craticula ambigua*	(Ehrenberg) D.G. Mann
CRA003	*Craticula buderi*	(Hustedt) Lange-Bertalot
CYM001	*Cymbella* cf. *affinis*	Kützing
CYM002	*Cymbella* sp.1	
DIA002	*Diatoma vulgaris*	Bory
DIS001	*Discostella pseudostelligera*	(Hustedt) Houk & Klee
DIS002	*Discostella stelligera*	(Cleve & Grunow) Houk & Klee
ENC001	*Encyonema silesiacum*	(Bleisch) D.G. Mann
ENC002	*Encyonopsis subminuta*	Krammer & E. Reichardt
EUN001	*Eunotia incisa*	Gregory
EUN002	*Eunotia subarcuatoides*	Alles, Nörpel & Lange-Bertalot
EUN003	*Eunotia rhomboidea*	Hustedt
EUN004	*Eunotia zygodon* var. *elongata*	Hustedt
EUN005	*Eunotia intermedia*	(Krasske ex Hustedt) Nörpel & Lange-Bertalot
EUN006	*Eunotia indica*	Grunow
EUN007	*Eunotia soleirolii*	(Kützing) Rabenhorst
EUN008	*Eunotia arcus*	Ehrenberg
EUN009	*Eunotia faba*	Ehrenberg
EUN010	*Eunotia boreoalpina*	Lange-Bertalot & Nörpel
EUN011	*Eunotia* sp.1	
EUN012	*Eunotia tenella*	(Grunow) Hustedt

EUN013	*Eunotia genuflexa*	Nörpel
EUN014	*Eunotia* cf. *julii*	Lange-Bertalot & Tagliaventi
EUN015	*Eunotia camelus*	Ehrenberg
EUN016	*Eunotia denticulata*	(Brébisson ex Kützing) Rabenhorst
EUN017	*Eunotia fennica*	(Hustedt) Lange-Bertalot
EUN018	*Eunotia cf. tropica*	Hustedt
EUN019	*Eunotia* sp.2	
EUN020	*Eunotia* cf. *compactarcus*	Lange-Bertalot, Pavlov & Kevkov
EUN021	*Eunotia* cf. *ursamaioris*	Lange-Bertalot & Nörpel
EUN022	*Eunotia* cf. *crassula*	Metzeltin & Lange-Bertalot
EUN023	*Eunotia paludosa*	Grunow
EUN024	*Eunotia bidens*	Ehrenberg
EUN025	*Eunotia bigibba*	Kützing
FRA001	*Fragilariforma telum*	(J.R. Carter & P. Denny) P.D. Almeida, C.E. Wetzel & E. Morales
FRU001	*Frustulia saxonica*	Rabenhorst
FRU002	*Frustulia* sp.1	
GOM001	*Gomphonema cf. gracile*	Ehrenberg
HAN001	*Hantzschia amphioxys*	(Ehrenberg) Grunow
KKR001	*Kurtkrammeria lacusglacialis*	(L. Bahls) L. Bahls
LUT001	*Luticola muticoides*	(Hustedt) D.G. Mann
LUT003	*Luticola intermedia*	(Hustedt) Levkov, Metzeltin & A. Pavlov
LUT004	*Luticola mutica*	(Kützing) D.G. Mann
LUT005	*Luticola acidoclinata*	Lange-Bertalot
LUT006	*Luticola hustedtii*	Levkov, Metzeltin & A. Pavlov
MAY001	*Mayamaea* cf. *atomus*	(Kützing) Lange-Bertalot
NAV001	*Navicula leptostriata*	Jørgensen
NEI001	*Neidium* cf. *ampliatum*	(Ehrenberg) Krammer
NIT001	*Nitzschia gracilis*	Hantzsch
PIN001	*Pinnularia viridiformis*	Krammer

PIN002	*Pinnularia brauniana*	(Grunow) Studnicka
PIN003	*Pinnularia socialis*	(Palmer) Hustedt
PIN004	*Pinnularia microstauron*	(Ehrenberg) Cleve
PIN005	*Pinnularia gibba*	(Ehrenberg) Ehrenberg
PIN007	*Pinnularia brandelii*	Cleve
PIN008	*Pinnularia inconstans*	Mayer
PIN009	*Pinnularia* sp.2	
PIN010	*Pinnularia* sp.3	
PIN011	*Pinnularia* sp.4	
PIN012	*Pinnularia* sp.5	
PIN013	*Pinnularia borealis*	Ehrenberg
PIN014	*Pinnularia* sp.6	
PIN016	*Pinnularia divergens*	W. Smith
PIN017	*Pinnularia divergentissima*	(Grunow) Cleve
RHO001	*Rhopalodia* cf. *operculata*	(C.Agardh) Håkanasson
SEL001	*Sellaphora pupula*	(Kützing) Mereschkovsky
SEL002	*Sellaphora* cf. *schadei*	(Krasske) C.E. Wetzel, L. Ector, B. Van de Vijver, Compère & D.G. Mann
STAU001	*Stauroneis phoenicenteron*	(Nitzsch) Ehrenberg
STAU002	*Stauroneis anceps*	Ehrenberg
UNK001	Unknown sp.1	

Supplementary Table 4. Supporting information for Figure 8. List of all operating coal and oil-fired power stations in Malaysia and Indonesia (Sumatra, Java, Kalimantan).

ID	Facility name	Country	Fuel type	Capacity (MW)	Year(s) of commissioning
1	Jimah	Malaysia	Coal	1400	2009
2	Manjung	Malaysia	Coal	3180	2002–2015
3	Mukah	Malaysia	Coal	270	2008–2009
4	PPLS	Malaysia	Coal	110	2006
5	Sejingkat	Malaysia	Coal	200	1997
6	Kapar	Malaysia	Coal	2420	1985–1994
7	Tanjung Bin	Malaysia	Coal	2100	2006–2007
8	Gelugor	Malaysia	Oil	398	2001
9	Melawa	Malaysia	Oil	50	1995
10	Sandakan	Malaysia	Oil	34	1999
11	Stratavest	Malaysia	Oil	60	1998
12	Tawau	Malaysia	Oil	36	1990
13	Bukit Asam	Indonesia	Coal	260	1989–1995
14	Paiton Baru	Indonesia	Coal	660	2012
15	Paiton I	Indonesia	Coal	1340	1999–2000
16	Paiton II	Indonesia	Coal	1320	1999–2000
17	Paiton III	Indonesia	Coal	815	2012
18	Paiton PLN	Indonesia	Coal	800	1993–1994
19	Ombilin	Indonesia	Coal	200	1996–1997
20	Suralaya	Indonesia	Coal	4025	1984–1997, 2011
21	Tanjung Awar Awar	Indonesia	Coal	700	2012–2013
22	Tanjung Jati-B	Indonesia	Coal	2640	2006, 2011-2012
23	Cirebon	Indonesia	Coal	660	2012
24	Cilacap Adipala	Indonesia	Coal	660	2014
25	Indramayu	Indonesia	Coal	990	2011
26	Pacitan	Indonesia	Coal	630	2013

27	Tarahan	Indonesia	Coal	200	2007–2008
28	Banten-Labuan	Indonesia	Coal	630	2009–2010
29	Banten-Lontar	Indonesia	Coal	945	2011–2012
30	Labuhan Angin	Indonesia	Coal	230	2008
31	Pelabuhan Ratu	Indonesia	Coal	1050	2013
32	Rembang	Indonesia	Coal	630	2011
33	Tambak Lorok	Indonesia	Oil	300	1970, 1983
34	Gresik	Indonesia	Oil	600	1986–1988
35	Gilimanuk	Indonesia	Oil	130	
36	Asam Asam	Indonesia	Coal	260	2000
37	Banjarsari	Indonesia	Coal	270	2015
38	Embalut	Indonesia	Coal	95	2014
39	Lati	Indonesia	Coal	14	
40	Tanjung Kasam	Indonesia	Coal	130	2012
41	Cikarang Listrindo	Indonesia	Coal	280	2017
42	Nagan Raya	Indonesia	Coal	220	2013–2014
43	Pangkalan Susu	Indonesia	Coal	440	2015
44	Sanggau	Indonesia	Coal	14	
45	Simpang Belimbing	Indonesia	Coal	300	2011
46	Teluk Sirih	Indonesia	Coal	224	2013